2003-12

The effects of isothermal deformation and annealing on the microstructure of nickel-aluminum-bronze in relation to the friction stir process

Vazquez, Brian K.

Monterey, California. Naval Postgraduate School

NAVAL POSTGRADUATE SCHOOL

MONTEREY, CALIFORNIA

THESIS

THE EFFECTS OF ISOTHERMAL DEFORMATION AND ANNEALING ON THE MICROSTRUCTURE OF NICKEL-ALUMINUM-BRONZE IN RELATION TO THE FRICTION STIR PROCESS

by

Brian Keith Vazquez

December 2003

Thesis Advisor: Terry McNelley

Approved for public release: distribution is unlimited

THIS PAGE INTENTIONALLY LEFT BLANK

REPORT DOCUMENTATION PAGE			Form Approved OMB No. 0704-0188
Public reporting burden for this collection of information is estimated to average 1 hour per response, including the time for reviewing instruction, searching existing data sources, gathering and maintaining the data needed, and completing and reviewing the collection of information. Send comments regarding this burden estimate or any other aspect of this collection of information, including suggestions for reducing this burden, to Washington headquarters Services, Directorate for Information Operations and Reports, 1215 Jefferson Davis Highway, Suite 1204, Arlington, VA 22202-4302, and to the Office of Management and Budget, Paperwork Reduction Project (0704-0188) Washington DC 20503.			
1. AGENCY USE ONLY ***(Leave blank)***	**2. REPORT DATE** December 2003	**3. REPORT TYPE AND DATES COVERED** Master's Thesis	
4. TITLE AND SUBTITLE: Miscrostructural Effects of Isothermal Deformation and Annealing on Nickel-Aluminum-Bronze Materials in Relation to the Friction Stir Process			**5. FUNDING NUMBERS**
6. AUTHOR(S) Brian K. Vazquez			
7. PERFORMING ORGANIZATION NAME(S) AND ADDRESS(ES) Naval Postgraduate School Monterey, CA 93943-5000			**8. PERFORMING ORGANIZATION REPORT NUMBER**
9. SPONSORING /MONITORING AGENCY NAME(S) AND ADDRESS(ES) N/A			**10. SPONSORING/MONITORING AGENCY REPORT NUMBER**
11. SUPPLEMENTARY NOTES The views expressed in this thesis are those of the author and do not reflect the official policy or position of the Department of Defense or the U.S. Government.			
12a. DISTRIBUTION / AVAILABILITY STATEMENT Approved for public release; distribution is unlimited			**12b. DISTRIBUTION CODE**

13. ABSTRACT (maximum 200 words)

The FSP of Nickel Aluminum Bronze is a novel approach to enhance the microstructural properties of the material through a shear deformation process. This thesis examines the effect on microstructure of isothermal annealing and quenching of as-cast Nickel Aluminum Bronze and, furthermore, reports on investigation of the effects of isothermal hot rolling on microstructure of this material. Quantitative analysis of the microstructure constituents shows that heating to about 800^{o}C results in the formation of beta by reversion of the eutectoid constituent alpha + kappa$_{iii}$. Further heating in the range of 800-1000^{o}C results in an approximately linear decrease in the volume fraction of primary alpha and a corresponding increase in the volume fraction of beta transformation products. Isothermal rolling of NAB over this same temperature interval results in deformation of both phases and an elongated, banded distribution of alpha and beta transformation products in the middle of this interval. This suggests that local peak temperature in the stir zone of material that has been subjected to FSP may be estimated by microstructure analysis. The yield and ultimate strengths of NAB are increased and ductility is also increased when rolled material is compared to as-cast NAB. However, strength and hardness appear to be independent of prior rolling temperature.

14. SUBJECT TERMS Friction Stir Processing, Nickel-Aluminum-Bronze, NAB, Isothermal Deformation, Annealing, Optical Microscopy, Naval Propellers, Surface Treatment, Thermo mechanically-Affected Zone, Shear Deformation, Lamellar tearing, Grain Growth, Homogenization of Microstructure			**15. NUMBER OF PAGES** 79
			16. PRICE CODE
17. SECURITY CLASSIFICATION OF REPORT Unclassified	**18. SECURITY CLASSIFICATION OF THIS PAGE** Unclassified	**19. SECURITY CLASSIFICATION OF ABSTRACT** Unclassified	**20. LIMITATION OF ABSTRACT** UL

NSN 7540-01-280-5500 Standard Form 298 (Rev. 2-89)
Prescribed by ANSI Std. 239-18

THIS PAGE INTENTIONALLY LEFT BLANK

Approved for public release: distribution is unlimited

THE EFFECTS OF ISOTHERMAL DEFORMATION AND ANNEALING ON THE MICROSTRUCTURE OF NICKEL-ALUMINUM-BRONZE IN RELATION TO THE FRICTION STIR PROCESS

Brian K. Vazquez
Lieutenant, United States Navy
B.S. Agricultural and Bio-Systems Engineering, University of Arizona, 1993

Submitted in partial fulfillment of the
requirements for the degree of

MASTER OF SCIENCE IN MECHANICAL ENGINEERING

from the

NAVAL POSTGRADUATE SCHOOL
December 2003

Author: Brian K. Vazquez

Approved by: Terry R. McNelley
Thesis Advisor

Anthony J. Healey
Chairman, Department of Mechanical and Astronautical Engineering

THIS PAGE INTENTIONALLY LEFT BLANK

ABSTRACT

The FSP of Nickel Aluminum Bronze is a novel approach to enhance the microstructural properties of the material through a shear deformation process. This thesis examines the effect on microstructure of isothermal annealing and quenching of as-cast Nickel Aluminum Bronze and, furthermore, reports on investigation of the effects of isothermal hot rolling on microstructure of this material. Quantitative analysis of the microstructure constituents shows that heating to about 800^{o}C results in the formation of beta by reversion of the eutectoid constituent alpha + kappa$_{iii}$. Further heating in the range of 800-1000^{o}C results in an approximately linear decrease in the volume fraction of primary alpha and a corresponding increase in the volume fraction of beta transformation products. Isothermal rolling of NAB over this same temperature interval results in deformation of both phases and an elongated, banded distribution of alpha and beta transformation products in the middle of this interval. This suggests that local peak temperature in the stir zone of material that has been subjected to FSP may be estimated by microstructure analysis. The yield and ultimate strengths of NAB are increased and ductility is also increased when rolled material is compared to as-cast NAB. However, strength and hardness appear to be independent of prior rolling temperature.

THIS PAGE INTENTIONALLY LEFT BLANK

TABLE OF CONTENTS

LIST OF FIGURES

LIST OF TABLES

THIS PAGE INTENTIONALLY LEFT BLANK

LIST OF ABBREVIATIONS, ACRONYMS, AND SYMBOLS

ASTM	American Society for Testing and Materials
BCC	Body Centered Cubic
CBN	Cubic Boron Nitride
DRX	Dynamically Recrystallized
EBSP	Electron Backscatter Pattern
EDS	Energy Dispersive Spectroscopy
FCC	Face Centered Cubic
FSP	Friction Stir Processing/Processed
HAZ	Heat-Affected Zone
KV	kilovolt
NAB	Nickel Aluminum Bronze
NSWCCD	Naval Surface Warfare Center, Caderock Division
OIM	Orientation Imaging Microscopy
OM	Optical Microscopy
PSN	Particle Stimulated Nucleation
RSC	Rockwell Science Center
SC	Simple Cubic
SEM	Scanning Electron Microscope
TMAZ	Thermo mechanically-Affected Zone
TWI	The Welding Institute
UNS	Unified Numbering System
Wt. %	Weight Percent

THIS PAGE INTENTIONALLY LEFT BLANK

ACKNOWLEDGMENTS

The author would like to thank the Defense Advanced Research Projects Agency (DARPA) for funding and support of this research; the Naval Surface Warfare Center (Carderock Division) for the NAB material and technical support; and Murray W. Mahoney at the Rockwell Science Center for his support and presentations.

The author would like to thank Professor Terry McNelley for providing the necessary direction for this research project.

The author would also like thank Charles Roe (NSWC-Carderock), K. Oishi, Chanman Park, Jesse Sherburn and current students in the FSP group for sharing their knowledge of the subject and in general… thanks.

Last but not least, the author would like to thank his family and friends for lending their patience, support and motivation.

THIS PAGE INTENTIONALLY LEFT BLANK

I. INTRODUCTION

A. NICKEL-ALUMINUM BRONZE

Nickel-aluminum bronze (NAB) refers to copper-based alloys with aluminum, nickel and iron as primary additions, with smaller amounts of manganese added as well. NAB alloys are used extensively for marine applications such as propellers, pumps, gears and valve components. NAB exhibits excellent corrosion resistance as well as good strength making it a material of choice for marine applications for naval surface and sub-surface platforms. In addition to its overall strength and corrosion resistance, NAB has other attributes. These include [Ref. 1] i) non-sparking behavior ii) good wear ability and low friction coefficients; iii) good fracture toughness at both elevated and lower temperatures; iv) high damping capacity to reduce noise transmissions; and v) exceptional resistance to fatigue which is a leading cause to material deterioration and failure in marine equipment.

The NAB alloy of interest here is designated as UNS C95800 and is commonly known as alpha nickel aluminum bronze or propeller bronze [Ref. 2]. NAB propellers for naval application are sand-cast IAW the ASTM B148 standard specification for aluminum bronze castings, and slow cooled to the atmosphere [Refs. 3-4]. The gradual cooling, which occurs at rates that vary with location in a cast propeller, plays an important role in determining the microstructure of as-cast NAB and directly affects the mechanical properties of the material [Refs. 5-6]. Also, during the solidification process gases come out of solution resulting in casting porosity and degrading the material's strength and corrosion resistance. [Ref 5]

Selective phase corrosion (de-alloying or de-aluminification) has been observed in corrosion tests on NAB materials that have had prolonged exposure in seawater [Refs.7-9]. It has been observed that repair welding of cast NAB introduces micro-structural defects and thermal stresses that adversely affect the corrosion resistance of the material. This behavior is especially noteworthy in association with weld repair of casting defects. Post welding heat treatments have been employed to alleviate the problems caused by welding.

Due to their size as-cast naval propellers cool very slowly, which results in a coarse microstructure. This results in a material that has lower yield strength when compared to more rapidly cooled cast material or material in a wrought condition. Current manufacturing processes favor the casting process to manufacture propellers although a more durable and wear-resistant surface condition would be desirable. Such property improvements are needed due to the high cavitation-erosion and corrosion attack that the propeller sees during operation, greatly reducing the service life of the component. Therefore, a satisfactory, low-cost procedure to refine the microstructure at the surface of an as-cast propeller while retaining or enhancing the strength and ductility of the material would be highly desirable for naval applications. FSP represents a viable means to accomplish such surface treatment and improve overall propeller performance.

B. FRICTION STIR PROCESSING (FSP)

FSP is a metal working process adapted from friction-stir welding [Ref. 8]. The technique uses a rotating tool that is pressed onto and traversed across the material surface to produce extreme plastic deformation as the tool "stirs" the material underneath it. The localized, severe plastic deformation and heating of the material homogenizes the microstructure and thereby improves material properties. The FSP tool consists of a cylindrical "shoulder" with a pin projection at its end that penetrates the material to the depth of the pin extension as the material is being processed. The shoulder interacts with the surface of the processed material to forge material softened by the intense deformation and adiabatic heating produced during FSP. What remains is a region of intense shear deformation with a fine-grained microstructure.

It is important to note that, although the intense plastic deformation may transfer material from one side of the tool to the other, FSP is a solid-state process, never melting the processed material. Studies on the effects of friction-stir processing on NAB as well as aluminum and magnesium alloys [Ref. 9-11] reveal that FSP improves material strength as well as ductility of material in the process zone, and this is desired for propeller application. It is possible that this process will find application not only in the repair of casting defects but also in altering future propeller designs due to the strengthening effect at the surface. However, a better understanding of the temperatures,

strains, and strain rates attained within the FSP stir zone is needed in order to better model the process and find the optimum processing parameters to achieve the desired microstructure. FSP provides the means to take an as-cast NAB microstructure and embed a wrought microstructure with localized modifications. This process would pave the way to optimize overall cost, material properties and increase the performance of the material in localize areas.

C. OBJECTIVES OF THIS RESEARCH

Adiabatic heating and severe plastic deformation during FSP result in steep gradients in temperature, strain and strain rate for the NAB material and it is difficult to separate the effects of heating and straining during analysis of stir zone microstructures. This thesis examines the results of isothermal annealing and quenching of as-cast NAB on microstructure and, furthermore, reports on an investigation into the effects of isothermal hot rolling on microstructure of NAB. Results will be compared to microstructure analysis of FSP stir zones. Results of tension testing on rolled NAB will be compared to results of such testing on as-cast material to assess the strengthening and hardening effects of rolling deformation. Finally, the thesis will seek to establish a basis in microstructure analysis to determine the distribution of peak temperatures within a FSP stir zone.

1. Annealing

NAB material was annealed at various temperatures ranging from 770^{o}C (0.7 T_m) to 1000^{o}C (0.94 T_m), followed by either cooling in air or by water quenching. Resulting cooling rates are estimated to be three- to six-orders of magnitude faster than encountered in casting of propellers. The microstructures are recorded to determine the effect of annealing and cooling on the coarse microstructure characteristic of as-cast and slowly cooled NAB material.

2. Hot Rolling

Conventional hot rolling, using a laboratory-scale rolling mill with reheating between each successive pass, was used to impart large strains into NAB samples at temperatures equivalent to those of the annealing study. Two different final thickness values were attained at each temperature of the study providing two strain amounts for

comparison. The effects on microstructures for both annealing and hot rolling could then be compared to stir zone microstructures in order to estimate the temperature, strain and strain rate values attained during FSP.

3. Hardness Testing

Rockwell B-scale hardness data was obtained for the as-cast, annealed, and hot rolled NAB to assess hardening relative to the as-cast NAB.

4. Tensile Testing

Tensile testing was used with flat, sheet-type samples machined from the hot rolled material as well as the as-cast NAB. The resulting data can be used to assess the effect of hot working on mechanical properties and lead to better predictive models of the effect of FSP on local properties in the stir zone.

II. BACKGROUND

In this chapter the constitution of NAB materials and their phase transformation characteristics will be discussed. This chapter will also provide more details of FSP and its effect on the microstructure of NAB materials.

A. COPPER-ALUMINUM AND DEVELOPMENT OF NICKEL-ALUMINUM BRONZE

Copper provides a basis for alloys that exhibit combinations of strength and corrosion resistance making them suitable for many marine applications. Cu-Al alloys that contain less than 7 wt% Al solidify as a single-phase face-centered cubic (fcc) solid solution alpha phase and will remain in this state upon cooling to room temperature. Alloys with more than 9.4 wt% Al will solidify as a single-phase body-centered cubic (bcc) solid solution beta phase. When the beta phase is allowed to cool slowly, the alpha phase will form from the beta until remaining beta phase undergoes a eutectoid reaction near 570^{o}C producing alpha + gamma.

The aluminum-rich gamma phase is anodic to the alpha phase. Therefore, the gamma phase preferentially corrodes and the alloy may experience dealuminization, which is similar in nature to dezincification of brass. [Ref. 9,17] Furthermore, it is recognized that alloys containing the gamma phase are less ductile as well as lower in strength than the NAB alloys [Ref. 9,17]. The additions of nickel and iron are known to extend the alpha phase field to allow for higher concentrations of Al without the formation of the gamma phase [Ref. 6,15]. Figure 2.1 represents a combination of three ternary diagrams: Cu-Al-Ni; Al-Ni-Fe; and Cu-Fe-Al, all at 500^{o}C, to show how the additions of Ni and Fe result in the suppression of gamma and substitution for it of various kappa phases containing Ni and Fe, which are known to increase the mechanical properties of NAB, in place of the gamma phase.

Increases of the aluminum content to values in the range of 8.8-10 wt% have been associated to an increase in strength, hardness and corrosion resistance [Ref.15], but also show a corresponding decrease in elongation which has been attributed to the kappa$_{iii}$

phase along grain boundaries [Ref.15]. NAB alloys containing about 9.5 wt% Al shows to have the best overall mechanical properties. Table 1 shows the NAB composition that was studied in this thesis.

Element	Cu	Al	Ni	Fe	Mn	Si	Pb
min-max	(min) 79.0	8.5-9.5	4.0-5.0	3.5-4.5	0.8-1.5	(max) 0.10	(max) 0.03
Nominal	81	9	5	4	1	-	-
Alloy	81.2	9.39	4.29	3.67	1.20	0.05	<0.005

Table 1: Composition (wt.%) of UNS C95800 NAB Material (Metals Hnbk, 9th Ed.) Bottom row represents composition of NAB alloy used in this study.

Alloys containing more than 3 wt% Fe exhibit a reduction in elevated temperature grain growth, in addition to reduced grain size and solidification range. A higher Fe content, up to 5 wt%, increases strength retention at elevated temperatures. A Fe content of 4 wt% was shown to give the optimum properties of wear, corrosion, abrasion, and fatigue resistance [Ref. 15].

The additions of Nickel in the range of 0 - 5 wt % result in grain refinement as well, and also provide an increase in hardness and strength by retarding the formation of the beta phase upon cooling. However, with a nickel content less than that of Fe the alloy may become susceptible to second phase attack in the presence of seawater, with a decrease in strength [Ref .15]. A nominal content of 5 wt % Ni and 4 wt % Fe was determined to be the ideal combination for maximum corrosion resistance [Ref. 15].

B. PHASES IN CAST NAB

NAB is a copper-based quaternary alloy with a further Mn addition as shown in Table 1. NAB has a nominal composition of 9 wt % Al and solidifies as the bcc beta phase as in the Cu-Al binary system. Upon further cooling the beta phase decomposes into four subsequent phases: an alpha fcc matrix and three kappa phases, designated as $kappa_{ii}$, $kappa_{iii}$ and $kappa_{iv}$. The $kappa_i$ only forms if the composition of iron is above 5 wt %. These kappa phases have been classified according to their individual

morphologies as seen in optical microscopy (OM) as well as the sequence in which they form from the beta phase [Refs 13-14].

1. Alpha Phase

The alpha phase is the equilibrium terminal solid solution with an fcc structure and a lattice perameter of a=3.64 Å [Ref. 18]. Proeutectoid alpha starts to form from the beta during cooling at about 1030^{o}C, and displays a Widmanstätten morphology in cast NAB cooled at a very slow rate. The alpha phase can be seen in Figure 2.2 as the light-etching phase. The alpha phase can form either intergranularly or intragranularly in the beta, but in more slowly cooled NAB it is seen to form as an intragranular alpha [Ref. 18].

2. Kappa$_{ii}$ Phase

There are four kappa phases observed in the as-cast NAB material: kappa$_i$ through kappa$_{iv}$ phases. The kappa$_i$ phase is not seen in Figure 2.2 because it is only observed when the iron content in NAB is greater than 5 wt. %. The kappa$_i$ particles have the same composition and structures as the kappa$_{ii}$ particles but they are coarser and dendritic in nature due to their formation at higher temperatures in higher iron content NAB. The kappa$_{ii}$ phase is a globular or dendritic, rosette-shaped structure found in NAB alloys [Refs. 18-19]. The kappa$_{ii}$ size can range from 5-10 μm with a nominal Fe_3Al composition. The kappa$_{ii}$ phase has a DO_3 crystal structure with a lattice parameter of a= 5.71 Å [Ref. 18]. The DO_3 crystal structure is an ordered bcc superlatice consisting of eight bcc cells in which the body centered atom alternates between Fe and Al, as seen in Figure 2.3. The kappa$_{ii}$ phase forms from the beta phase at about 950^{o}C. The alpha phase may begin to form in the same vicinity. The NAB phase diagram and phase transformation diagram is shown in Figure 2.4.

3. Kappa$_{iii}$ Phase

The kappa$_{iii}$ phase, with a NiAl composition, may initially form as a globular particle but mainly precipitates as a fine, lamellar constituent along the alpha/beta interface. It has also been known to form as a crust-like structure around kappa$_{ii}$ particles. The kappa$_{iii}$ phase has a B2 crystal structure with a lattice parameter of a = 2.88 Å, which is approximately half the lattice parameter of the kappa$_{ii}$ phase [Ref. 18]. The B2 structure for NiAl is an ordered CsCl type crystal structure and it is hypothesized to form

initially on the $kappa_{ii}$ particles which act as substrates for the growth of $kappa_{iii}$ [Ref. 20]. The $Kappa_{iii}$ starts to form at about 800°C (Figure 2.4).

4. $Kappa_{iv}$ Phase

The $kappa_{iv}$ particles are fine, cruciform precipitates formed in the alpha matrix beginning at about 850°C, as indicated in Figure 2.4. The $kappa_{iv}$ particle consists of the same Fe_3Al composition and DO_3 structure as $kappa_{ii}$ particles and the $kappa_{iv}$ has a lattice parameter of a= 5.77 Å, which is similar to that of $kappa_{ii}$.

5. Beta Phase

The beta phase has a bcc structure. Upon equilibrium cooling, beta will transform to alpha and the various kappa particles. At higher cooling rates and lower transformation temperatures the rate of beta decomposition is slower and any remaining beta upon reaching room temperature is termed "retained beta or beta prime" having either a 3H or 2R martensite structure [Refs. 18-19].

Upon casting NAB to form a large component various microstructures are encountered because of the very slow but variable cooling rates. In general, the final product will have a coarse, heterogeneous microstructure and varying mechanical properties due to the heterogeneity and porosity. These factors lead to lower material strength and reduced cavitation and corrosion resistance. Propellers, which are made from NAB, operate in a harsh environment in which their service life is diminished by cavitation and corrosion damage. For this reason it is desirable to eliminate inherent defects that arise due to casting without changing the manufacturing process. FSP provides a viable solution by improving the properties of cast NAB thereby extending the service life.

C. FRICTION STIR PROCESSING (FSP)

FSP is an outgrowth of the principles of friction stir welding (FSW) which was developed by The Welding Institute (WTI) in 1991 [Ref. 31]. In FSP the tool is used to process material in the absence of joining two pieces of metal. FSP "stirs" the metal with the motion of a tool to create a more homogenous and refined microstructure with improved mechanical properties.

FSP uses a non-consumable tool that rotates at various speeds; the process may be accomplished by the use of a modified milling machine. The tool is typically made of a heat-resistant steel and consists of a cylindrical shoulder of approximately 25mm in diameter and a centrally located, smaller concentric pin at the tool end. The pin geometry can vary but is typically either threaded, with or without flutes or stepped, and is approximately 6-10mm in diameter and 6-12mm in depth. The rotating tool is forced into the fixed material to be processed until the tool shoulder touches the surface of the material. The tool then traverses along the material surface in a single or multiple pass fashion. The tool shoulder diameter and the pin depth will determine the area and depth of the surface treatment. The rotating tool and pin, through a combination of sticking and sliding friction, impart severe plastic deformation and adiabatic heating on a column of material beneath the tool shoulder and pin. The tool shoulder acts like a barrier to prevent lifting the material displaced by the pin, resulting in a stirring action in the material. The heating softens the material to the point were an equilibrium is reached between the heat generated from adiabatic deformation conditions and the heat lost by convection and conduction to the environment around the stir zone. It needs to be emphasized that FSP is a solid-state process and melting does not occur; as temperature increases in the stir zone, the material's strength decreases leading to reduced heat generation by adiabatic deformation. On this basis, temperature increases may be self-limited. The process is illustrated in the schematic of Figure 2.6. Once the tool has processed the material, three distinct areas are established: 1) a stir zone (sometimes referred to as "the nugget"), 2) a thermo-mechanically affected zone (TMAZ), 3) Base metal. Figure 2.5 distinctly shows each area.

Immediately around the pin is an area called the stir zone or nugget which undergoes intense plastic deformation that results in a fine, equiaxed, defect free microstructure with areas of varying microstructures. The stir zone represents a processed area that is expected to exhibit better mechanical properties than the base metal. These improved properties can be attributed to the fine grain size attained in the stir zone, which can be as fine as about 3 μm [Ref. 10]. Tensile testing done by the Rockwell Science

Center (RSC) of specimens from the stir zone showed improvements in the yield and ultimate strengths of the material as well as an improvement in ductility, as seen in figure 2.7.

Just below the stir zone is the TMAZ, which is a region that undergoes less severe plastic deformation and heating effects than the stir zone. The length of the TMAZ is typically 200 to 400 μm before there is a transition into the base metal which experiences no plastic deformation except at the boundary and undergoes little heating effects. Therefore, the TMAZ experiences moderate strain, strain rate and temperature gradients and exhibits shear during FSP [Ref. 30]. Consequently, the TMAZ may still show improved mechanical properties.

The base metal located underneath the TMAZ is relatively unaffected except for heating effects near the boundary between the two areas. The base metal retains all the defects from casting and has the same properties as the as-cast NAB.

The mechanical properties and microstructure of NAB that have undergone FSP vary throughout the stir zone and TMAZ due to local variations in temperature, cooling rates, strain and strain rates. The effects of FSP on the microstructure remain to be clarified because of the simultaneous effects of all these factors. Therefore, it is helpful to consider the effects of isothermal annealing and isothermal hot rolling deformation separately on NAB microstructures.

FSP may become an important future material-processing step in future manufacturing operations intended to improve the mechanical characteristics of metallic components. Before it can be implemented in manufacturing environments a complete understanding of the process is needed. In order to accomplish this task both extensive experimentation and modeling of the process needs to be done and verified against each other to achieve accurate predictions of the effect of FSP on microstructure and mechanical properties of NAB.

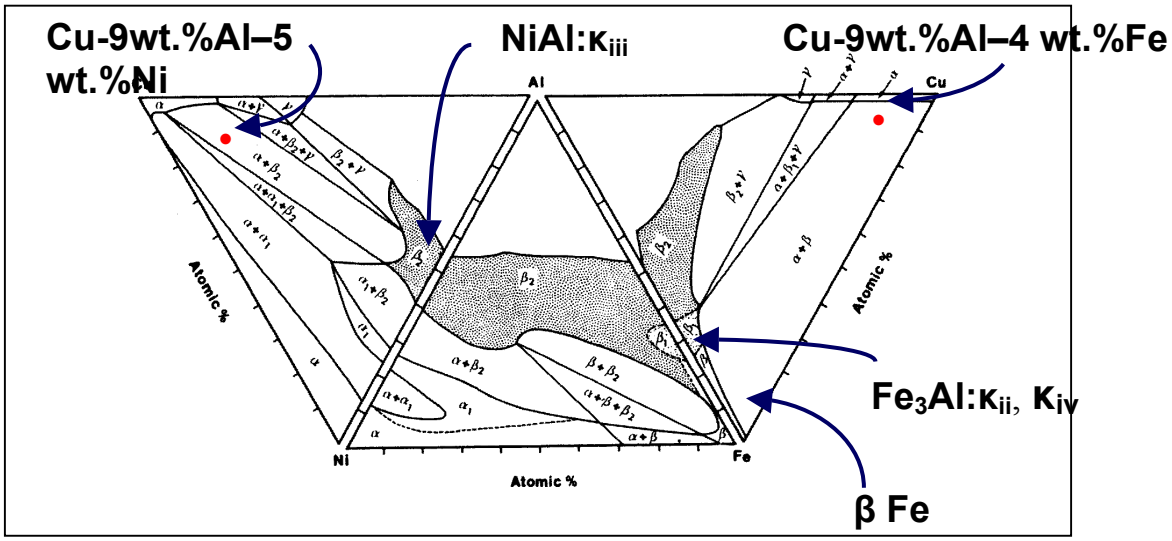

Figure 2.1: Quaternary equilibrium NAB phase diagram. F. Hasan, A. Jahanafrooz, G.W. Lorimer and N. Ridley, Metall. Trans. A., vol. 13A (1982) pp. 1337-45. (*Modified courtesy T. R. McNelley.*)

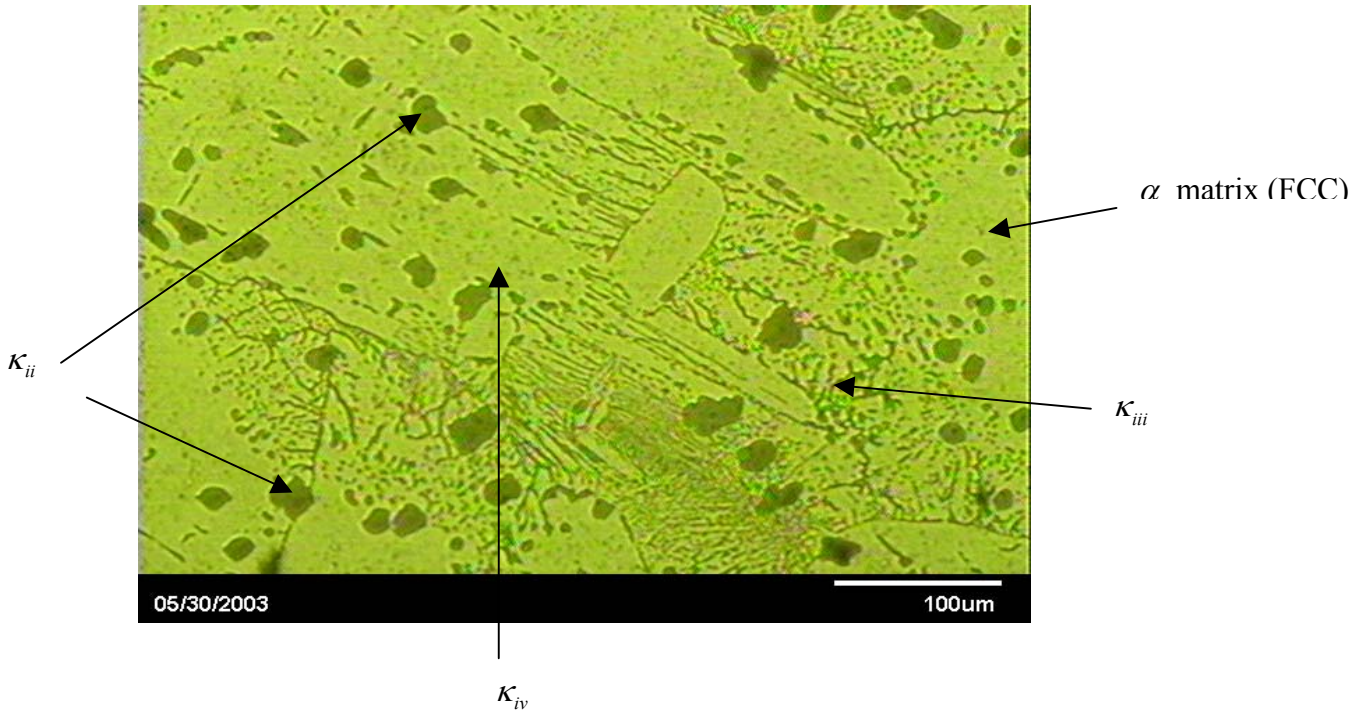

Figure 2.2: Optical micrograph of 380°C annealed NAB at 370x. showing the alpha and kappa phases. [Ref. 30]

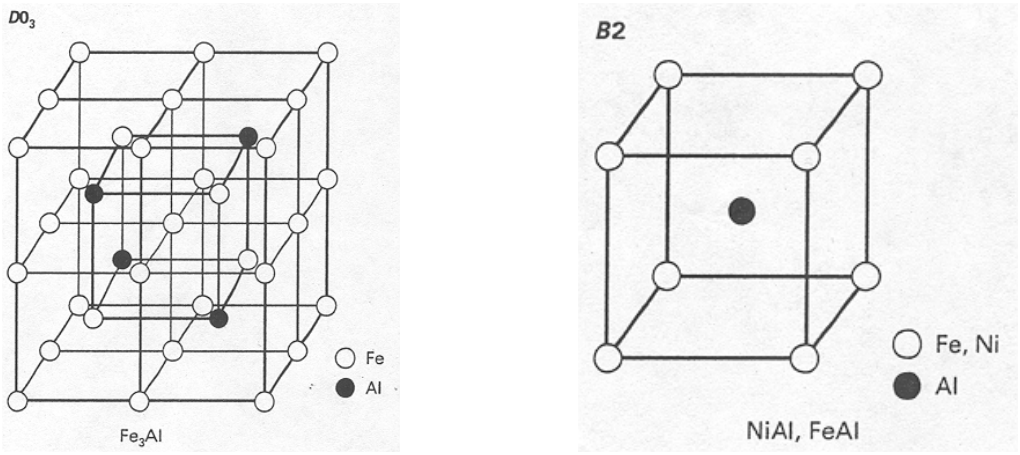

Figure 2.3: DO_3 and B2 crystal structures. $Kappa_{ii}$ and $kappa_{iv}$ have a Fe_3Al composition with a D03 crystal structure, while $kappa_{iii}$ has a NiAl composition with a B2 crystal structure. [Ref. 18]

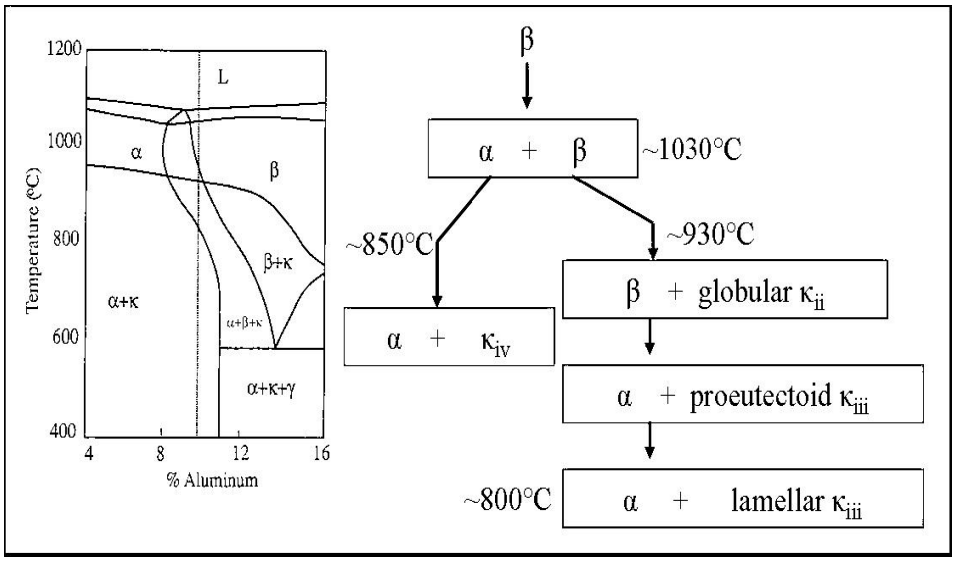

Figure 2.4: NAB phase diagram with corresponding transformation diagram. [Refs. 16&23]

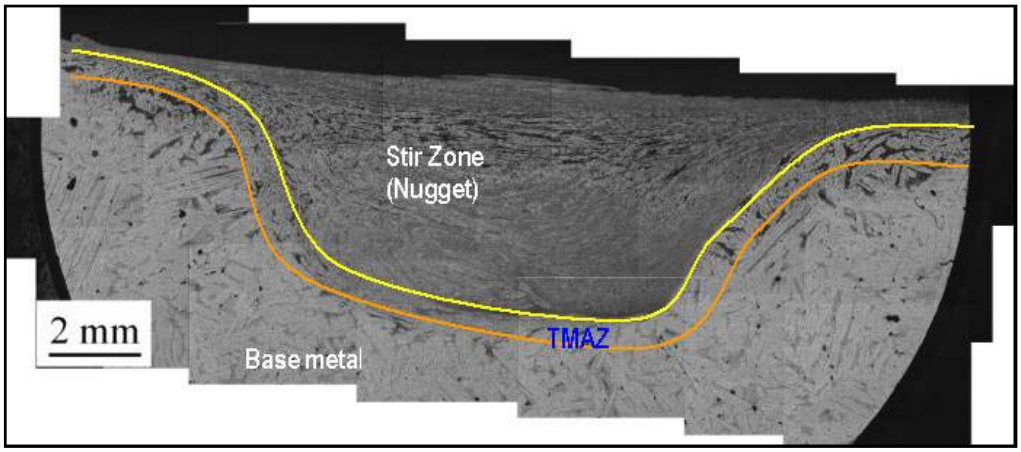

Figure 2.5: FSP region. (*Courtesy K. Oishi, NPS)*

Figure 2.5 is a montage which shows: the stir zone characterized by extensive plastic deformation, the TMAZ which experiences both large plastic deformations and heating effects, and the base metal which remains relatively unchanged from the as-cast condition, experiencing little deformations and heating effects.

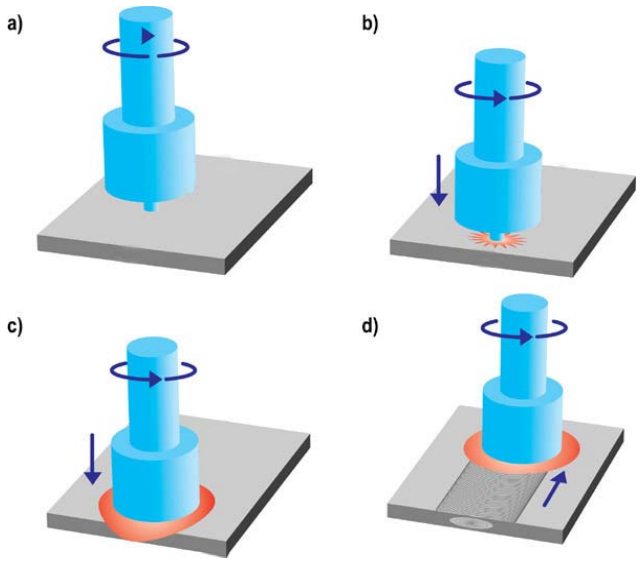

Figure 2.6: Friction Stir Process (Courtesy M. W. Mahoney, RSC)

Figure 2.6 shows FSP from a) to d). The process involves lowering the rotating tool with a certain force to allow the pin to plunge into the metal to be processed until the shoulder of the tool is reached as depicted in picture “c” above. The tool then traverses across the surface of the material leaving a wake of processed material behind.

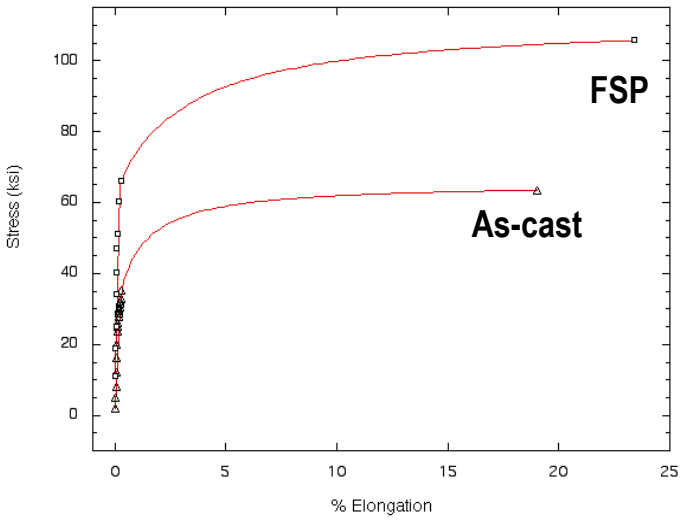

Yield Strength (ksi)		Tensile Strength (ksi)
FSP	62.8	107.8
As-cast	31.2	64.8

Figure 2.7: Stress vs strain plot for FSP vs As-Cast NAB tensile samples (data and graph courtesy of M. Mahoney)

THIS PAGE INTENTIONALLY LEFT BLANK

III. EXPERIMENTAL

A. EXPERIMENTAL PROCEDURES

1. Samples Material

The samples examined in the course of this experiment were fabricated from a plate of as-cast NAB that had been sectioned from a propeller casting and supplied by the Naval Surface Warfare Center – Carderock Div., Washington, D.C.. This material had also been used in research conducted by Nabach [Ref. 25]. Specimens were machined locally. The rolling billets were all of dimensions about 4.4 x 3.12 x 1.85cm(1.73 × 1.23 × 0.73 inches), which represents the samples' length, width and height.

2. Rolling Procedure

Previous attempts at rolling reported by Cuevas [Ref. 10] and Nabach [Ref. 25] were unsuccessful in that severe 'alligator' cracking after reductions of 10 – 20% was encountered at all temperatures up to 650ºC. This is consistent with the data shown in Figure 3.1 below. The cracking appeared to follow the lamellar alpha + $kappa_{iii}$ structure. Thus, isothermal rolling was conducted here at temperatures near and above the eutectoid at temperature, i.e., at temperatures ranging from 780^{o}C to 1000^{o}C, in an attempt to avoid cracking problems. The objective was to impart two different strain values on the NAB specimens by rolling the billets to either a 10:1 or a 3.5:1 reduction. After rolling was completed and samples mounted, a comparison of the microstructures of the isothermally deformed NAB samples to the annealed NAB samples (annealed microstructure analysis provided by Sherburn, [Ref. 20]) was the next step.

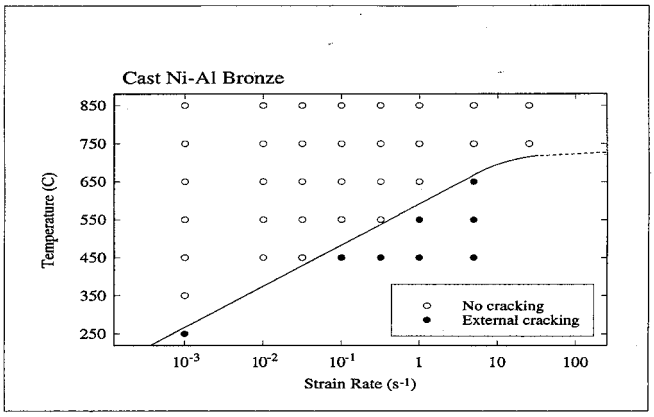

Figure 3.1: External Cracking diagram. [Ref. 24]

Prior the initial rolling pass each billet was annealed for one hour in a NEY 2-160 series II furnace. The preheating temperatures were 780, 820, 870, 900, and 1000°C as measured by the installed thermocouple. The temperature indicated by the installed thermocouple was compared to that measured by a hand held thermometer using a K-type thermocouple and adjustments were made to attain ± 5ºC accuracy of temperature control. A steel plate placed on the furnace hearth to act as a heat sink to help stabilize and maintain the temperature within the furnace. After equilibration at the desired rolling temperature the billet was transferred from the furnace to a FENN laboratory two-high, pull over, rolling mill and rolled with a reduction of one tenth the original thickness on each pass until the final thickness was attained. The sample was returned to the furnace for 5 minutes between each pass and the time to transfer the sample from the furnace to the rolling mill was about 10 seconds. A reduction schedule is shown in Tables 3a and 3b and initial and final sample billet size data is shown in Table 4.

3. Instron Tensile Procedures

Tensile test specimens were fabricated as shown in Figure 3.3. They were mounted separately between wedge grips with a 12.5 mm (0.5 in.) Instron extensometer attached. The test parameters were inputted into the Instron software. The parameters that were selected are as follows: U.S. customary units were selected for the output data, the crosshead speed for each test pull was set at 1.3 mm m^{-1} (0.05 in m^{-1}), the sampling rate

for the machine was set at 1 point s^{-1}, and switch over from extensometer to crosshead displacement measurement was set at 1.0 %. Before each run the extensometer was calibrated using existing functions. Once all the appropriate settings were made then each sample was pulled to failure and the data were copied to disk. The output data were force and displacement for each sample point. It is important to note that caution needs to be taken to ensure that the samples are mounted tightly in the wedge grips to avoid slipping and also to ensure the sample is correctly aligned.

4. Rockwell Hardness Testing Procedure

Hardness data was taken from the undeformed grip areas of the tensile specimens. The Rockwell machine was used on the 'B' scale using a 100 kg weight to determine the hardness. Hardness values were collected from each sample, and, depending on the consistency of the values obtained, either 4 or 5 hardness values were taken from each sample and averaged. The averaged results are shown in Table 4.

5. Sample Preparation

a. Sectioning

All samples were initially sectioned using a manual hacksaw with a flexible high strength steel blade. The samples were mounted in a tabletop vise and cut to obtain a representative sample, which was taken towards the middle of the rolled billet as shown in Figure 3.2 below.

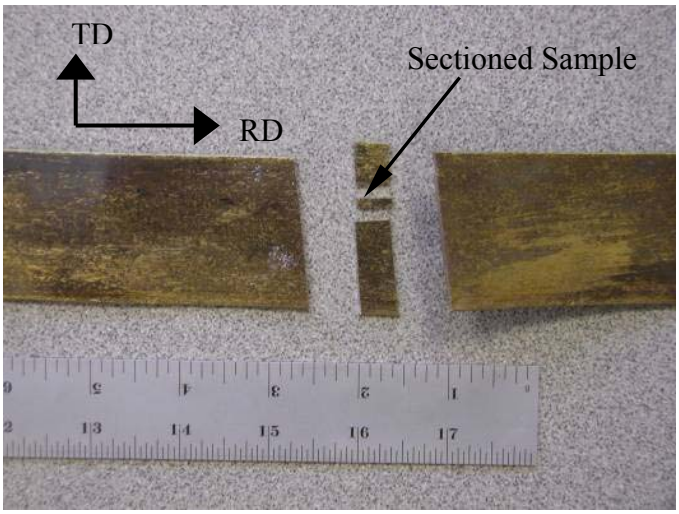

Figure 3.2: Sectioned sample of a billet rolled at 900°C to a 10:1 reduction. RD represents roll direction and TD represents transverse direction.

b. Polishing

Mechanical polishing of the samples was accomplished in the steps outlined in Table 3.1 below. Water was used as the lubricant for the silicon carbide (SiC) paper. Grinding was done in one direction until the sample was flat and the scratches were all in one direction. This process usually took about 15 seconds for grits 240, 320, 400, and 600, which were fixed to a stationary metal plate. The sample was then rotated 90^{o} and the process repeated two more times. The grinding force used was about 30 N.

Mechanical polishing was continued on SiC paper on a rotating wheel with the following grits: 800, 1000, 2400 and 4000. Water was used as the lubrication medium. The sample was ground and rotated as described above with a downward force of about 20 N. Once the samples were ground and rotated twice a smaller force of about 10 N was used and gradually lessened until the sample was hydroplaning across the surface of the SiC paper. After each grinding step the sample was rinsed with water and ethanol or methanol. Once finished with SiC paper polishing the sample was placed in an ultrasonic ethanol or methanol bath for 15 minutes to remove any residual particles.

The final steps of polishing were accomplished on polishing wheels with 3 and then 1 μm Metadi oil-based diamond suspension and finished using Mastermet Colloidal Silica Polishing Suspension polishing agents. The samples were rotated in a direction that opposed the rotation of the polishing wheel to create random cutting of the surface. The optical microscope was used to determine if residual scratches were present from previous steps.

Step	Abrasive	Time	RPM
1	240 grit SiC	2 Min	N/A
2	320 grit SiC	1 Min	N/A
3	400 grit SiC	1 Min	N/A
4	600 grit SiC	1 Min	N/A
5	800 grit SiC	2 Min	120
6	1000 grit SiC	1 Min	120
7	2400 grit SiC	1 Min	120
8	4000 grit SiC	1 Min	120
9	3 μm OBDS	20 Min	50
10	1 μm OBDS	20 Min	50
11	Colloidal Silica	25 Min	50

Table 2: Polishing Table showing grits and times. OBDS stands for oil based diamond suspension.

c. Etching

The etching solution used was a 10% Ammonium-persulfate solution in water. After polishing was completed the sample was etched for 15 seconds and rinsed with water and ethanol and air-dried. The OM was used to determine if more etching was needed.

d. Microscopy

All samples were examined using optical microscopy techniques. The Zeiss JENOPHOT 2000 inverted light microscope with an installed Pulnix TMC-74 digital camera and associated SEMICAPS digital imaging software provided the micrographs. A calibrated micron bar was included in each micrograph. The micron bar was further modified to be able to identify it more clearly with the use of Photoshop 7.0 software. All micrographs were obtained using the 1x additional magnification lens of the microscope

e. Tensile Samples

Tensile samples were fabricated from the rolled specimens in accordance with ASTM 8 standards following the guidelines of Standard Test Methods for Tensile Testing of Metallic Materials. The test specimen size fell under the sub size category. The dimensions of the sample were: overall length 101.6 mm (4 in), length of reduced section 31.8 mm (1.25 in), length of grip section 31.8 mm (1.25 in), width of grip section 9.5 mm (0.375 in), radius of fillet 6.3 mm (0.25 in), and width of gauge section 6.3 mm (0.25 in). Thickness of the specimen shall have a maximum of 6.3 mm (0.25 in). The specimens were fabricated by the NPS machine shop.

B. EXPERIMENTAL DATA

1. Rolling Data

NAB billets were rolled with reheating between passes at temperatures of 780, 820, 870, 900, and 1000^{o}C with a reduction schedule as shown in Tables 3a and 3b. The thickness of the billet was measured after each pass and the billet was returned to the furnace for reheating at the appropriate temperature. A reduction corresponding to one-tenth the original thickness of the billet was sought. This reduction amount was maintained as much as possible, but because of mill spring back adjustments were required. Table 3a shows the reductions for the sample reduced by 10:1 overall and Table 3b shows the reductions for the sample reduced 3.5:1 overall. Including the as-cast material there were 11 samples overall. Only one billet was rolled at each temperature. The initial and final billet size was measured and is shown in Table 4. The rolling mill was operated at 18.5 rpm with a roller diameter of 109.5 mm (4.23 in).

Pass #	1000°C Sample		900°C Sample		870°C Sample		820°C Sample		780°C Sample	
	T(in.)	R (in.)	T (in.)	R (in.)	T (in.)	R (in.)	T (in.)	R (in.)	T (in.)	R (in.)
0	0.734	0.05	0.735	0.065	0.735	0.057	0.732	0.051	0.732	0.051
1	0.684	0.08	0.670	0.072	0.678	0.099	0.681	0.091	0.681	0.096
2	0.604	0.084	0.598	0.074	0.579	0.064	0.590	0.082	0.585	0.074
3	0.520	0.097	0.524	0.103	0.515	0.079	0.508	0.075	0.511	0.071
4	0.423	0.053	0.421	0.049	0.436	0.066	0.433	0.061	0.440	0.079
5	0.370	0.07	0.372	0.042	0.370	0.087	0.372	0.084	0.361	0.076
6	0.300	0.099	0.330	0.140	0.283	0.055	0.288	0.073	0.285	0.065
7	0.201	0.048	0.190	0.030	0.228	0.075	0.215	0.064	0.220	0.067
8	0.153	0.073	0.160	0.088	0.153	0.071	0.151	0.065	0.153	0.060
9	0.08		0.072		0.082		0.086		0.093	

Table 3a: Roll reduction data for NAB at 1000°C, 900°C, 870°C, 820°C, and 780°C with a 10:1 reduction to an approximate true strain value of 2.3.

Pass #	1000°C Sample		900°C Sample		870°C Sample		820°C Sample		780°C Sample	
	T(in.)	R (in.)	T (in.)	R (in.)	T (in.)	R (in.)	T (in.)	R (in.)	T (in.)	R (in.)
0	0.734	0.033	0.730	0.058	0.735	0.063	0.732	0.06	0.733	0.052
1	0.701	0.10	0.672	0.096	0.672	0.072	0.672	0.091	0.681	0.096
2	0.601	0.091	0.576	0.074	0.600	0.095	0.581	0.071	0.585	0.074
3	0.510	0.08	0.502	0.047	0.505	0.075	0.510	0.06	0.511	0.068
4	0.430	0.074	0.455	0.105	0.430	0.062	0.450	0.076	0.443	0.082
5	0.356	0.066	0.350	0.072	0.368	0.063	0.374	0.086	0.361	0.073
6	0.290	0.08	0.278	0.06	0.305	0.083	0.288	0.077	0.288	0.068
7	0.21		0.218	0.012	0.222	0.021	0.211		0.22	
8			0.206		0.201					

Table 3b: Rolling reduction data for NAB at 1000°C, 900°C, 870°C, 820°C, and 780°C with a 3.5:1 reduction and an approximate true strain value of 1.26.

		Initial Values (in.)			Final Values (in.)		
Roll Temp(C)	Approx. Strain	Length	Width	Thickness	Length	Width	Thickness
780	1.26	1.698	1.23	0.733	5.165	1.450	0.220
820	1.26	1.64	1.231	0.732	5.025	1.465	0.211
870	1.26	1.72	1.231	0.735	5.17	1.566	0.201
900	1.26	1.598	1.23	0.73	4.652	1.559	0.206
1000	1.26	1.686	1.23	0.734	5.065	1.633	0.21
780	2.3	1.738	1.228	0.732	N.A.	N.A.	N.A.
820	2.3	1.642	1.23	0.732	11.063	1.554	0.086
870	2.3	1.625	1.219	0.735	12.688	1.563	0.082
900	2.3	1.64	1.23	0.732	14.533	1.654	0.072
1000	2.3	1.797	1.231	0.734	13.164	1.802	0.08

Table 4: Initial and final dimensions of the rolled specimens at the for the various isothermal rolling conditions.

Table 4 above indicates data were not available (N.A.) for the 780^{o}C sample. Measurements were not attainable for this sample because the sample underwent severe splitting on the last pass as shown in Figure 3.3.

Figure 3.3: NAB 780^{o}C sample rolled to a 10:1 reduction.

2. Tensile Data

The raw displacement and force data obtained from the Instron machine and subsequent modification of the data to show stress and strain values were omitted from this report. The initial and final gauge length data for the tensile specimens were collected to calculate percent elongation. Table 5 shows a consolidation of this data along with initial and final values of gauge thickness and width. Tensile samples from material rolled at 1000°C to both strain values were not fabricated or tested due to schedule constraints.

Sample Description	Initial X-Sectional Area(in^2)	Initial Values (in.)			Final Values (in.)		
		Gauge Length	Width	Thickness	Gauge Length	Width	Thickness
Strain of Approximately 1.26							
NAB, 780°C	0.0254	1.317	0.254	0.100	1.441	0.238	0.093
NAB, 820°C	0.025654	1.328	0.254	0.101	1.465	0.24	0.092
NAB, 870°C	0.022927	1.322	0.227	0.101	1.406	0.218	0.095
NAB, 900°C	0.02525	1.308	0.25	0.101	1.464	0.236	0.093
Strain of Approximately 2.3							
NAB, 780°C	0.017424	1.320	0.242	0.072	1.331	0.24	0.071
NAB, 820°C	0.021983	0.315	0.247	0.089	1.315	0.247	0.089
NAB, 870°C	0.017112	1.321	0.248	0.069	1.325	0.245	0.066
NAB, 900°C	0.016575	1.324	0.255	0.065	1.327	0.253	0.062

Table 5: Initial and final dimensions of the tensile sample gauge dimensions.

3. Hardness Data

Rockwell hardness data was obtained from tensile samples at various temperatures and rolling strain values. Hardness data for these conditions is shown in Table 6 below. The Rockwell hardness 'B' scale value for the as cast NAB sample was 36.

Rolling Deformation Temperature in ^{o}C	Rockwell Hardness value for NAB w/ 3.5:1 Reduction	Rockwell Hardness value for NAB w/ 10:1 Reduction
780	56.8	65.4
820	58.25	68.63
870	57.75	69.5
900	57	69.5
1000	58.25	67.25

Table 6: Rockwell Hardness values, 'B' scale for rolled NAB

IV. RESULTS AND DISCUSSION

This chapter will present a summary of the data obtained from rolling, tension testing, and microscopy and then provide observations on the implications of the data.

A. ROLLING STUDY

By rolling at temperatures such that the eutectoid constituent reverts to the high temperature phase, i.e., alpha + $kappa_{iii}$ → beta, large strains were attained in the NAB, providing material for analysis of the effect of isothermal deformation on microstructure. The billets were rolled to two final nominal strain values of 1.26 and 2.3 at temperatures listed in Tables 7 and 8. . The amount of strain and the strain rate during each pass are provided in the tables that follow. The von Mises equivalent strain in fully rolled materials is given in Table 11.

Pass #	1000°C Sample	900°C Sample	870°C Sample	820°C Sample	780°C Sample
	Strain	Strain	Strain	Strain	Strain
0					
1	-0.07055	-0.09259	-0.08072	-0.07222	-0.07222
2	-0.12438	-0.11369	-0.15784	-0.14344	-0.15195
3	-0.14975	-0.1321	-0.11714	-0.14964	-0.13524
4	-0.20646	-0.21886	-0.16652	-0.15974	-0.14959
5	-0.13387	-0.12374	-0.16414	-0.15184	-0.1979
6	-0.20972	-0.1198	-0.26806	-0.25593	-0.23639
7	-0.40048	-0.55207	-0.2161	-0.29232	-0.25886
8	-0.27287	-0.17185	-0.39891	-0.35336	-0.36319
9	-0.64841	-0.79851	-0.62372	-0.56293	-0.49784

Table 7: Strain value per pass through the rolling mill for 10:1 reduction.

Pass #	1000°C Sample	900°C Sample	870°C Sample	820°C Sample	780°C Sample
	Strain	Strain	Strain	Strain	Strain
0					
1	-0.04600	-0.08279	-0.08961	-0.08552	-0.07358
2	-0.15391	-0.15415	-0.11333	-0.14551	-0.15195
3	-0.16418	-0.13751	-0.17237	-0.13034	-0.13524
4	-0.17063	-0.0983	-0.16077	-0.12516	-0.1428
5	-0.18885	-0.26236	-0.1557	-0.18499	-0.20469
6	-0.20505	-0.23031	-0.18777	-0.2613	-0.22592
7	-0.32277	-0.24313	-0.31763	-0.3111	-0.26933
8		-0.05662	-0.09937		

Table 8: Strain value per pass through the rolling mill for 3.5:1 reduction.

Pass #	1000°C Sample	900°C Sample	870°C Sample	820°C Sample	780°C Sample
	Strain Rate (1/sec)	Strain Rate (1/sec)	Strain Rate (1/sec)	Strain Rate (1/sec)	Strain Rate (1/sec)
0					
1	0.89	1.02	0.95	0.90	0.90
2	1.24	1.19	1.41	1.34	1.38
3	1.46	1.37	1.31	1.47	1.40
4	1.87	1.92	1.67	1.64	1.58
5	1.64	1.58	1.80	1.73	1.99
6	2.24	1.65	2.56	2.49	2.42
7	3.59	4.16	2.60	3.05	2.86
8	3.51	2.80	4.11	3.94	3.96
9	6.77	7.59	6.60	6.23	5.73

Table 9: Strain rate data per pass through the rolling mill for 10:1 reduction.

Pass #	1000°C Sample	900°C Sample	870°C Sample	820°C Sample	780°C Sample
	Strain Rate (1/sec)	Strain Rate (1/sec)	Strain Rate (1/sec)	Strain Rate (1/sec)	Strain Rate (1/sec)
0					
1	0.71	0.97	1.01	0.98	0.91
2	1.37	1.40	1.19	1.36	1.38
3	1.53	1.43	1.58	1.38	1.40
4	1.70	1.28	1.66	1.44	1.54
5	1.96	2.28	1.76	1.89	2.02
6	2.25	2.42	2.11	2.51	2.36
7	3.22	2.80	3.11	3.16	2.91
8		1.46	1.93		

Table 10: Strain rate data per pass through the rolling mill for 3.5:1 reduction.

Nominal Reduction	T_{roll} (°C)	ε_x	ε_y	ε_z	$\varepsilon_{VonMises}$
3.5:1	780	0.165	1.112	-1.204	1.345
	820	0.174	1.120	-1.244	1.374
	870	0.241	1.101	-1.297	1.403
	900	0.237	1.069	-1.265	1.366
	1000	0.283	1.100	-1.251	1.380
10:1	780	N.A.	N.A.	N.A.	N.A.
	820	0.234	1.907	-2.140	2.348
	870	0.249	2.055	-2.193	2.462
	900	0.296	2.182	-2.319	2.611
	1000	0.381	1.991	-2.216	2.452

Table 11: True strain values for rolled billet in the x, y, and z (width, length, and thickness) directions with overall Von Mises equivalent strains.

These strain histories are typical of laboratory-scale rolling and may be useful in simulations of this rolling process and for comparison to thermomechanical histories calculated for FSP. Maximum values for strain and strain rates were typically attained from the last roll pass unless an additional pass was needed to help facilitate straightening of the sample. This can be seen in the last pass for the 3.5:1 reduction samples at 870 and 900^{o}C. Equivalent von Mises strain values of about 1.4 and 2.4 were calculated for reduction schedules of 3.5:1 and 10:1, respectively.

B. HARDNESS RESULTS

Data from Table 6 shows that the ambient temperature hardness of the NAB increases as hot rolling strain increases. NAB undergoes a hardness increase of about 58% for the 3.5:1 reduction sample and an increase of about 88% for the 10:1 reduction sample. It is noteworthy that the hot rolling temperature has little apparent effect on the ambient temperature hardness value. A decreasing hardness would be expected for increase rolling temperature due to increased recovery effects and microstructure coarsening that would produce softening.

C. TENSILE TESTING RESULTS

The stress verses strain data were plotted for as-cast and rolled NAB for both nominal reductions values of 3.5:1 and 10:1. The resulting stress-strain plots are shown in the figures below.

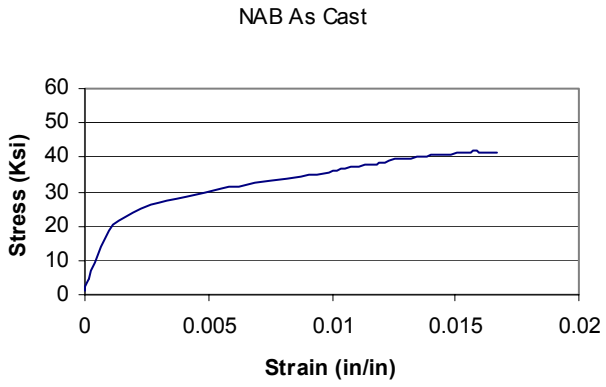

Figure 4.1: Stress vs. Strain for As-Cast NAB

Figure 4.1 shows stress-strain data for the as-cast NAB sample. The data suggests a low-ductility in as cast material and yield strength of about 186.2 MPa (27 Ksi) and

ultimate strength of 289.7 MPa (42 Ksi) in association with a strain to failure of only 0.017. The yield and tensile strength data are consistent with earlier reports for as-cast NAB (see Figure 2.7) although the strain to failure is only one-tenth that in the RSC data. This difference may be attributable to the fact that only one as-cast specimen was tested, precluding assessment of specimen-to-specimen variability.

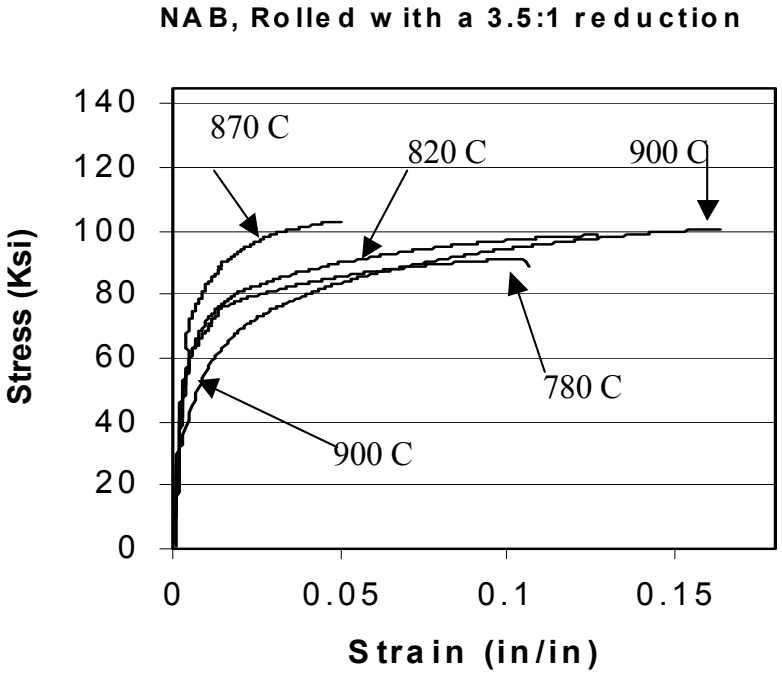

Figure 4.2: Stress vs. strain curves for rolled NAB with a 3.5:1 reduction at various temperatures.

Figure 4.2 shows stress strain plots for NAB that has undergone a 3.5:1 reduction in thickness during rolling at several of the temperatures indicated in Table 4. The graph shows that hot rolling lead to an increase in yield and ultimate strength when compared to the as-cast NAB accompanied by an increase in strain to failure. For example, for rolling at 820^{o}C both the yield and ultimate strength values were over 100 % greater than corresponding values for as-cast material. Furthermore, the strain-to-failure value increased by almost ten-fold over that for as-cast material. From the data, an increase in yield strength and a decrease in strain to failure with decreasing hot rolling temperature may be noted, with the exception of the data for 870ºC. This inconsistency can be

attributed to tensile sample flaws and/or inability to test multiple samples at the same temperature to attain repeatability.

Figure 4.3 shows that there is a further increase in strength over the as-cast condition in material rolled to larger hot rolling strain. However, these data, especially the ductility, are considered unreliable due to lack of straightness and of surface cracking observed during the latter rolling passes. Also, some problems were encountered with preloading and localized yielding outside the gauge length of the extensometer due to these factors. Appendix B provides picture of the tensile samples and illustrates their condition.

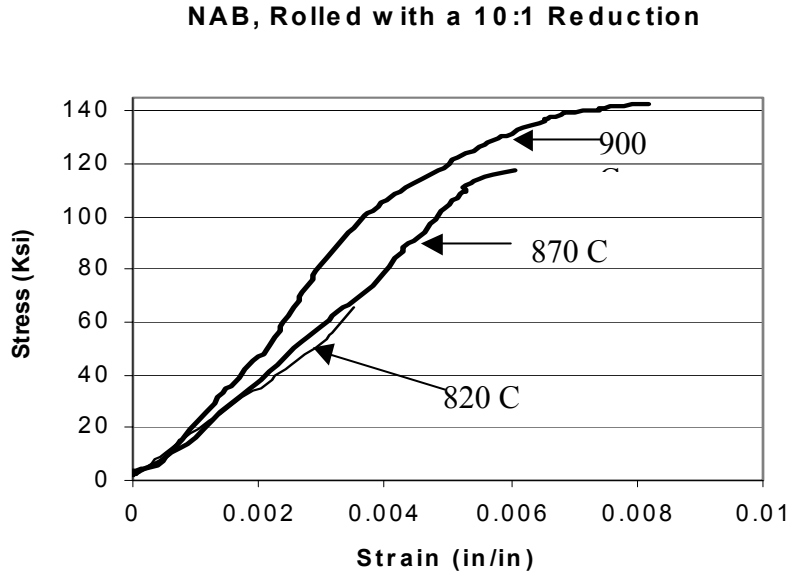

Figure 4.3: Stress strain curves for rolled NAB with a 10:1 reduction at various temperatures.

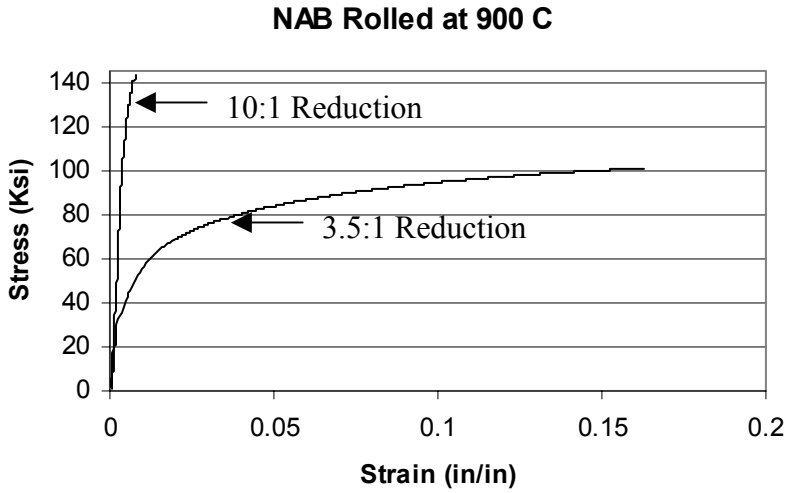

Figure 4.4: Stress strain curves for rolled NAB with 3.5:1 and 10:1 reductions at 900^{o}C.

Figure 4.4 shows a comparison of the yield strengths between the 3.5:1 and the 10:1 reduction 900^{o}C samples. From the graph a 40% increase in ultimate strength is noticed with the higher strained sample. Similar results can be ascertained by comparing Figures 4.2 and 4.3.

D. MICROSCOPY RESULTS

Figure 4.4 compares the microstructures of samples that have experienced only annealing, followed either by water quenching or air-cooling, to the rolled NAB for both nominal strains of 1.26 and 2.3. Appendix A provides additional micrographs for reference.

Examination of these micrographs shows that increasing heating temperature results first in reversion of the eutectoid constituent according to the reaction alpha + $kappa_{iii}$ → beta. As the heating temperature increases above the eutectoid the relative fraction of primary alpha decreases while that of the beta increases. Depending on the subsequent cooling rate, the primary alpha is retained to room temperature while the beta transforms. In samples that have experienced only heating and annealing, the transformation products of the beta appear to be mainly martensite during cooling at high rates associated with water quenching (WQ). In samples subjected to air-cooling after annealing (AC) the transformation products of the beta appear to be Widmanstätten alpha

as well as bainite and martensite. This difference is most apparent when materials annealed at 1000°C are compared. In both cases the structure was apparently 100% beta prior to cooling.

The apparent volume fractions of transformed beta and alpha are equivalent for the same heating temperature when annealed materials are compared to hot rolled materials. The effect of the rolling deformation is to cause shape change in the various phases, i.e. elongation of both the alpha and beta regions are apparent for rolling temperatures of 820, 870 and 900ºC, and the degree of elongation increases as the rolling strain increases from 1.4 to 2.4. Thus, it appears that the fractions of alpha and beta are dependent only on temperature and not on the strain.

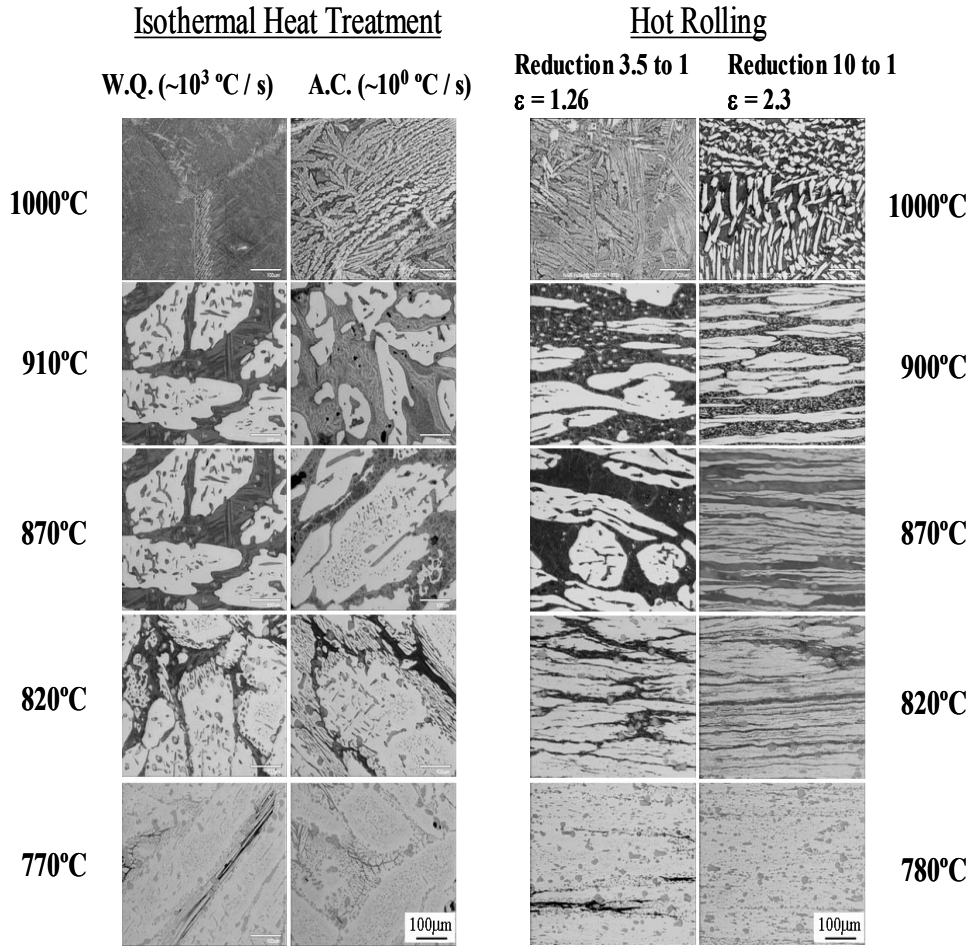

Figure 4.4: Micrographs of annealed and hot rolled NAB at various temperatures (annealed micrographs courtesy of Jesse Sherburn).

The morphology of the Widmanstätten alpha for material rolled to a 10:1 reduction at 1000^{o}C (in Figure 4.4) is relative coarse and this suggests that transformation may have begun during the transfer from the furnace to the rolling mill in this sample, i.e., as the sample thickness becomes reduced it is increasingly difficult to maintain isothermal deformation conditions. The higher cooling rate in the relative thin material after exiting the roll gap in this condition resulted in subsequent transformation of the remaining beta to martensite. In contrast, the material rolled to a reduction of 3.5:1 cooled less upon transfer to the mill and cooled more slowly after exiting the roll gap due to the greater thickness, resulting in a mixture of Widmanstätten alpha and bainite.

Figure 4.5 shows a comparison of the deformed NAB at nominal strain values of both 1.26 and 2.3 to the stir zone in material after FSP stir zone. The FSP material had been designated 516 and was processed with a tool rotation rate of 800 rpm and traversing rate of 152 mm m^{-1} (6 in m^{-1}). For the larger rolling strain of 2.3 the microstructure similarities for some rolling temperatures to locations in the stir zone are obvious. From this comparison an inference can be made that the stir zone temperatures in such locations may be estimated by comparison to the results for annealing and isothermal deformation of this work. In particular, temperatures of 900^{o}C or more were attained in the stir zone, and the appearance of band-like features in the stir zone likely reflects deformation of a two-phase alpha + beta microstructure to strain values in excess of 2.3.

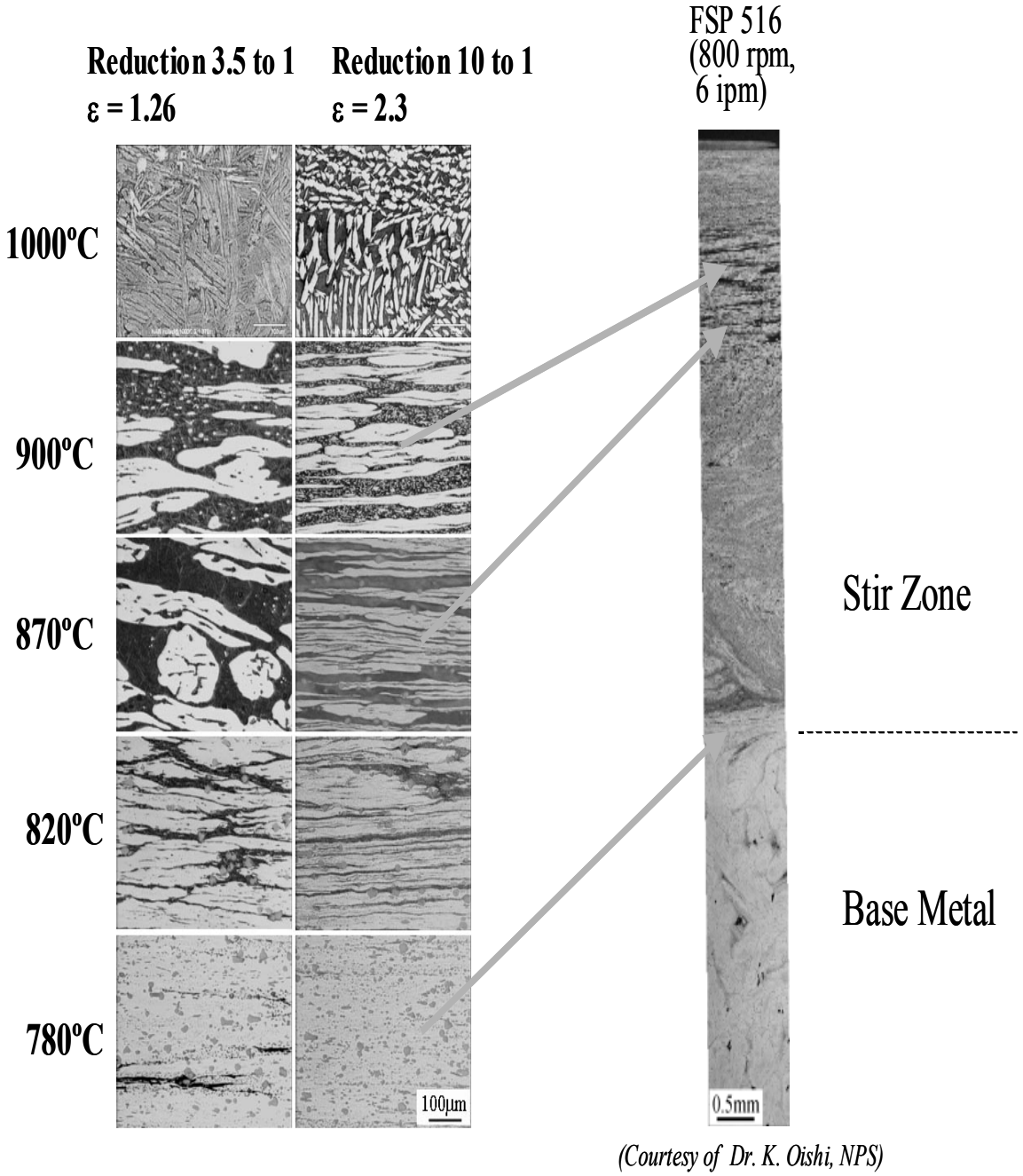

Figure 4.5: Micro-structural comparison of deformed NAB to the stir zone.

The volume fractions of alpha and transformed beta appear to be a function mainly of temperature and not of strain. This suggests that the relative fractions of these

constituents in stir zones after FSP may enable estimation of local temperatures. This is potentially very useful since direct temperature measurement, e.g. by insertion of a thermocouple into material undergoing FSP, is impossible due to the severe deformation associated with this process.

Information on the volume fraction of both constituents was obtained by analyzing the micrographs at each temperature and strain value with the use of photo-enhancing software and a Matlab code to conduct the pixel count. Appendix C provides the Matlab code to count the pixels associated with α and transformed beta. Appendix D provides the data tables in which the following figures of percent volume fraction of each constituent with temperature are plotted according to strain history.

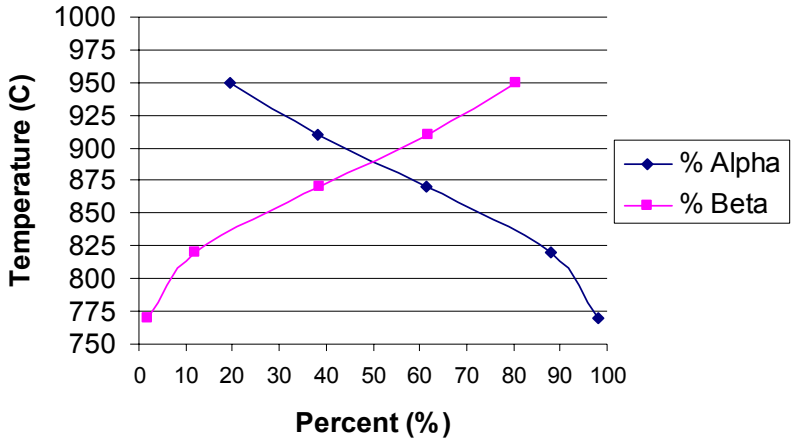

Figure 4.6: Plot of percent volume fraction of alpha and transformed beta with temperature of non-deformed annealed NAB.

The above figure shows an increasing fraction of beta with increasing temperature and a corresponding decrease of the alpha. This trend is seen with all the plots at all temperatures and strain values. When determining the volume fractions the $kappa_{ii}$ was lumped with transformed beta and the $kappa_{iv}$ was lumped with the alpha phase.

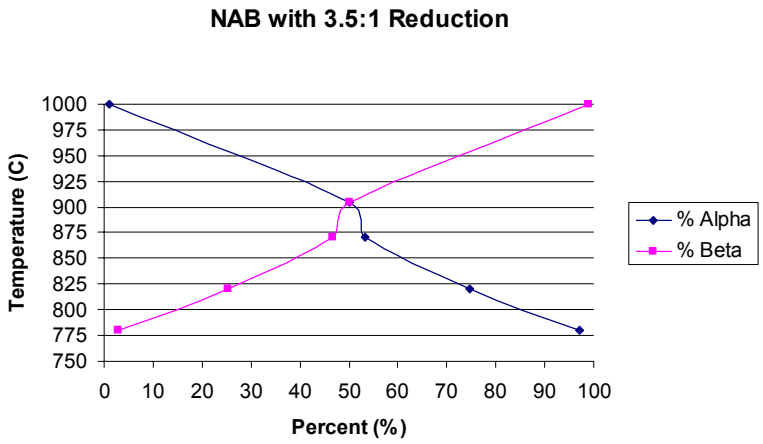

Figure 4.7: Plot of percent volume fraction of alpha and transformed beta with temperature of 3.5:1 hot rolled NAB.

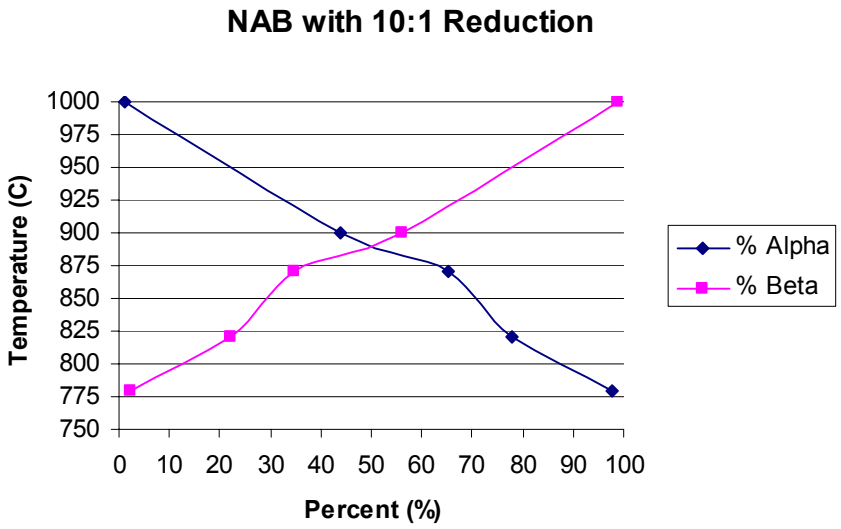

Figure 4.8: Plot of percent volume fraction of alpha and transformed beta with temperature of 10:1 hot rolled NAB

THIS PAGE INTENTIONALLY LEFT BLANK

V. SUMMARY AND CONCLUSION

FSP provides the ability to selectively refine the microstructure of a material thereby converting from a cast to a wrought microstructure without changing its shape. Peak temperatures in the stir zone have been difficult to ascertain. This thesis provides a means to estimate temperatures within the stir zone by analysis of the microstructures of as-cast, annealed, and hot rolled NAB for two different strain values. Hardening and strengthening effects were also determined due to the hot rolling process. The following conclusions were drawn from the information and data collected:

1. Surface cracking and severe alligator cracking occurs when rolling NAB at temperatures around 780^{o}C with a 10:1 reduction in thickness. Nabach also noted this type of cracking for lower deformation temperatures and the cracking was associated with the presence of brittle kappa$_{iii}$ constituent particles in the microstructure. At 820^{o}C and above the NAB could be readily rolled to a 10:1 reduction in thickness. Some surface cracking was always noted but became less apparent at higher rolling temperatures.

2. Annealing NAB at temperatures varying from 770^{o}C to 1000^{o}C showed the presence of a two-phase phase region wherein increasing temperature resulted in increased fraction of beta. Upon hot rolling NAB at temperatures varying from 780^{o}C to 1000^{o}C the alpha and beta phases were able to deform compatibility with each other. At temperature of 1000ºC, the microstructure consisted of all beta and the equiaxed appearance of the material rolled at this temperature suggests that dynamic recrystalization occurs during rolling. At a 1000^{o}C rolling temperature and a 10:1 reduction Widmanstätten alpha phase forms during transfer from the annealing furnace to the rolling mill because of convective and conductive losses during this process.

3. Comparison of the hot rolled NAB to the FSP stir zone micro-structural features from the rolled samples can be correlated to areas of the FSP stir zone. By this comparison estimates can be made for the temperatures and strains involved within the FSP stir zone.

4. Comparing the micrographs of annealed to deformed NAB at various temperatures there is a direct correlation between the fractions of primary alpha,

transformed beta and temperature. This phenomenon is essentially the lever rule applied to the appropriate phase diagram. From this data, a plot of percent transformed beta versus temperature for all strain values may be plotted. Temperature within a FSP stir zone can be estimated within this range from if the volume fraction of transformed beta is known. This is apparently independent of the amount of deformation that NAB has undergone. Figure 5.1 shows this correlation.

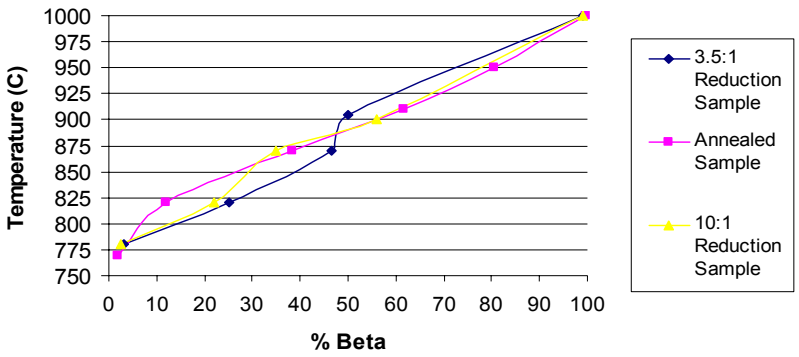

Figure 5.1: Percent beta vs. temperature for annealed(non-deformed) and deformed samples.

5. From the tensile testing experiments mechanical properties of the rolled NAB showed an increase in yield and ultimate tensile strength and elongation over the as-cast NAB. Table 12 summarizes this data. Figure 5.2 shows an increase in ultimate tensile strength with an increase in strain.

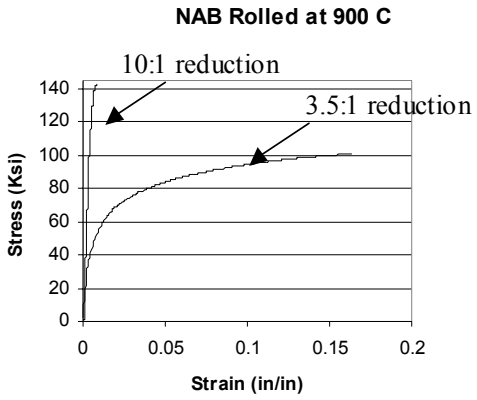

Figure 5.2: Stress vs. strain for NAB rolled at 900°C with 3.5:1 and 10:1 reductions.

Sample Condition	σ_y (Ksi)	σ_{uts} (Ksi)	%EL$_{ext}$	%EL$_{meas.}$	True Strain ε
As-Cast	27	42	1.7	4	0.0429
3.5:1 Reduction sample					
780 °C	60	91	11	9.4	0.09
820 °C	60	99	12	10.3	0.098
870 °C	52	103	--- **	6.4	0.062
900 °C	35	100	16.5	11.9	0.0113
10:1 Reduction sample					
780 °C	23	99	3.3	0.8	0.0083
820 °C	--- **	66	0.3	0.0	0.0
870 °C	--- *	118	0.6	0.3	0.003
900 °C	--- *	143	0.8	0.2	0.002

Table 12: Yield and ultimate strength and elongation data for tensile samples (* Unable to obtain yield stress due to localized strain outside extensometer gauge length. ** Unable to obtain %EL or yield stress due to early break at fillet because of pre-loading or surface cracking).

FSP is new technology to refine the microstructure of a material. With the aid of modeling exact predictions can be made of the final microstructure needed to provide the desired mechanical properties. The results for this thesis can be used to help refine the model predictions by correlating model results to experimentation.

THIS PAGE INTENTIONALLY LEFT BLANK

APPENDIX A

A. ANNEALED NON-DEFORMED MICROGRAPHS:

1000°C micrographs:

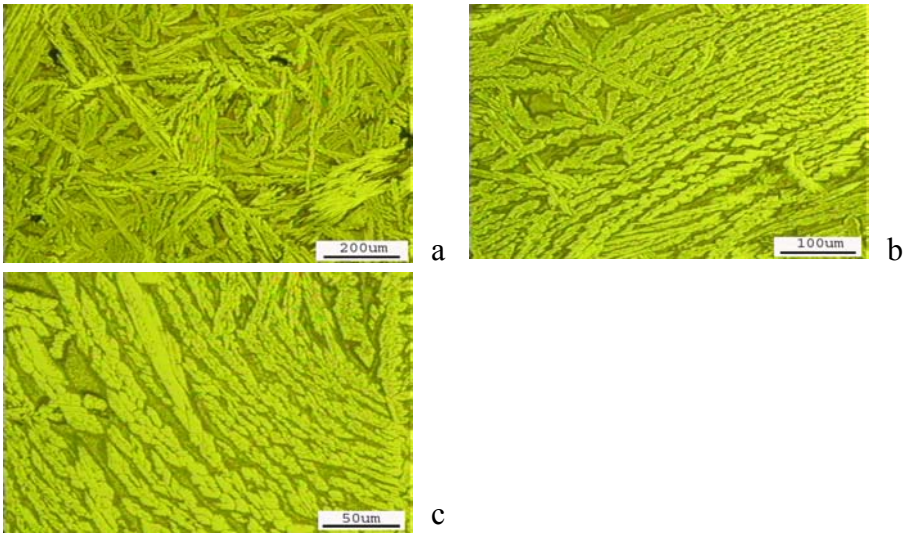

Figure A.1: The following micrographs (a through c) are for magnifications of 290x, 370x, and 750x at 1000°C, respectively.

910 °C micrographs:

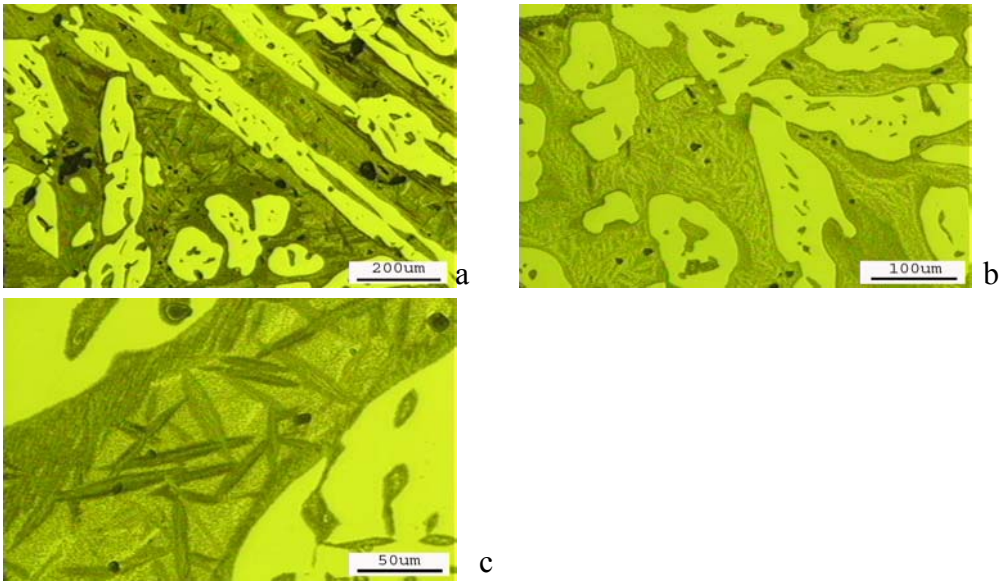

Figure A.2: The following micrographs (a through c) are for magnifications of 290x, 370x, and 750x at 910°C, respectively.

870°C micrographs:

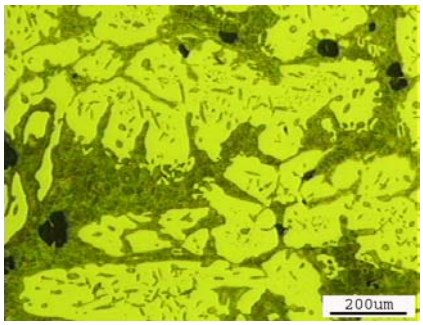

a

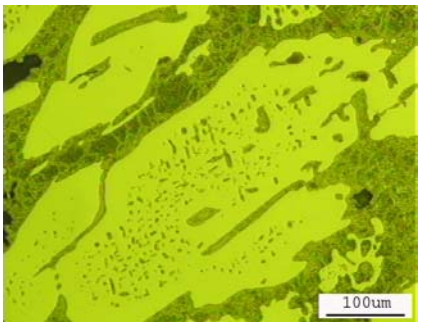

b

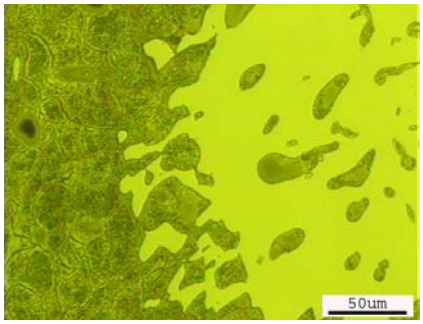

c

Figure A.3: The following micrographs (a through c) are for magnifications of 290x, 370x, and 750x at 870°C, respectively.

820°C micrographs:

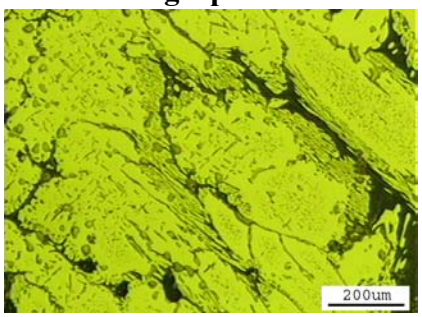

a

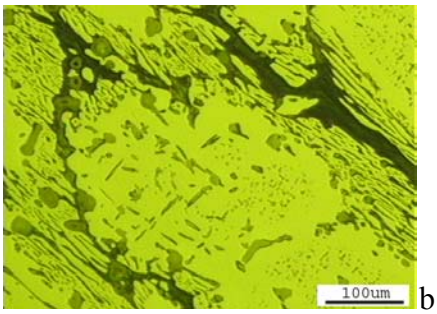

b

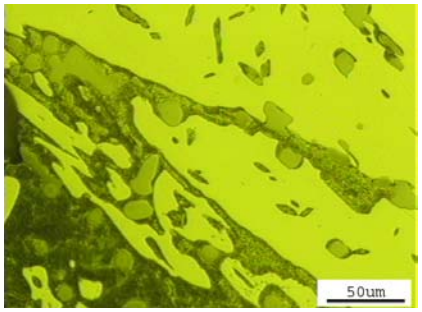

c

Figure A.4: The following micrographs (a through c) are for magnifications of 290x, 370x, and 750x at 820°C, respectively.

770°C micrographs:

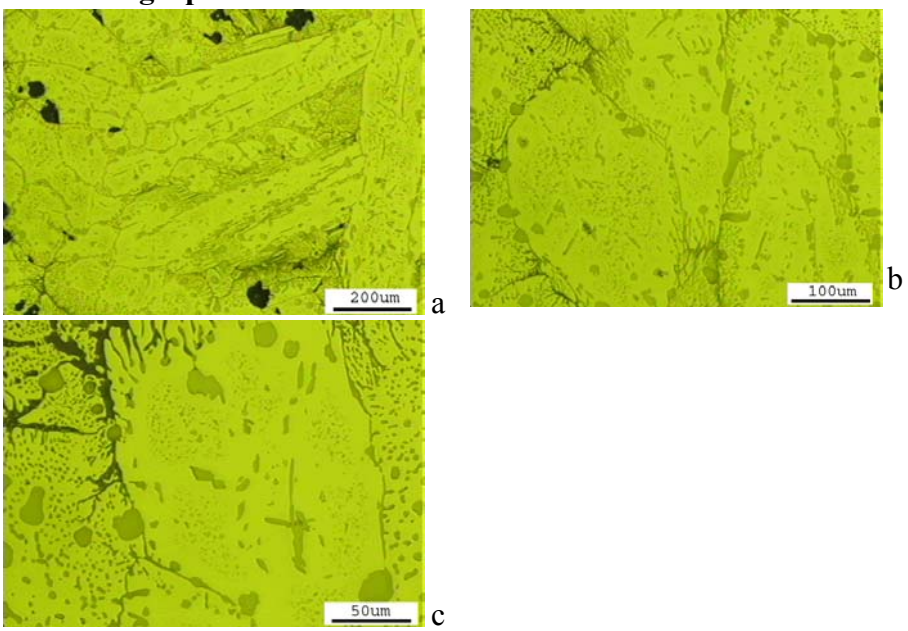

Figure A.5: The following micrographs (a through c) are for magnifications of 290x, 370x, and 750x at 770°C, respectively.

B. ANNEALED 3.5:1 DEFORMED MICROGRAPHS:

1000°C micrographs:

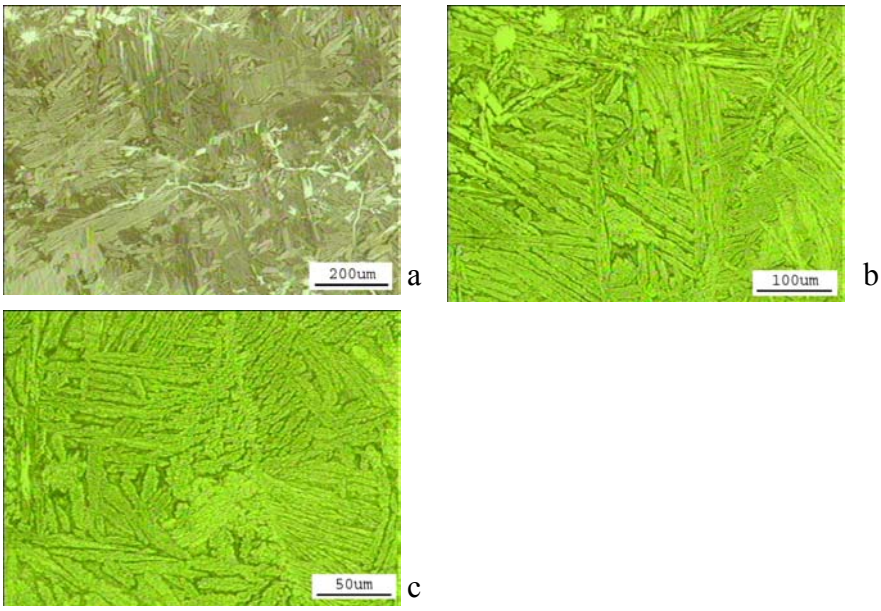

Figure A.6: The following micrographs (a through c) are for magnifications of 290x, 370x, and 750x at 1000°C, respectively.

900°C micrographs:

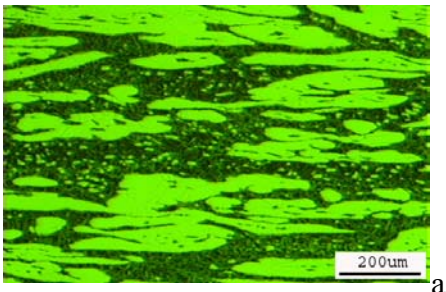

a

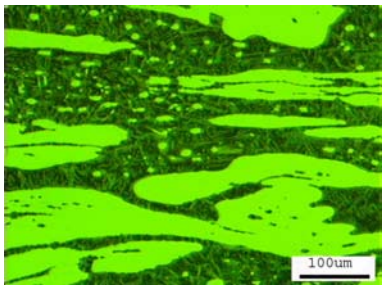

b

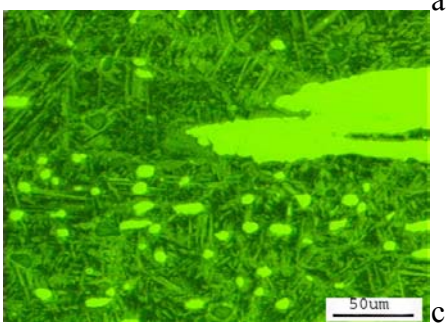

c

Figure A.7: The following micrographs (a through c) are for magnifications of 290x, 370x, and 750x at 900°C, respectively.

870°C micrographs:

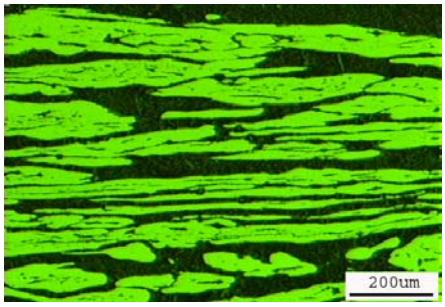

a

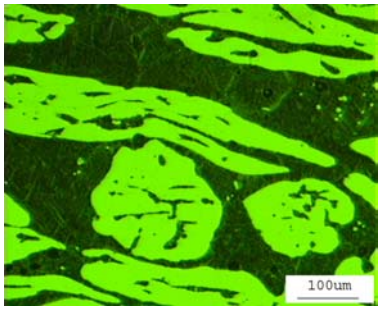

b

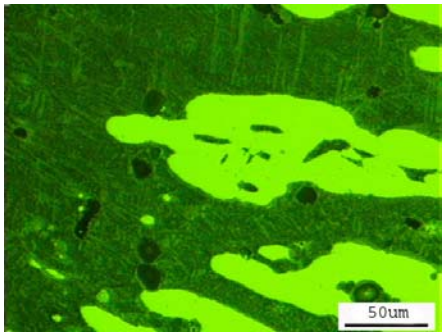

c

Figure A.8: The following micrographs (a through c) are for magnifications of 290x, 370x, and 750x at 900°C, respectively.

820°C micrographs:

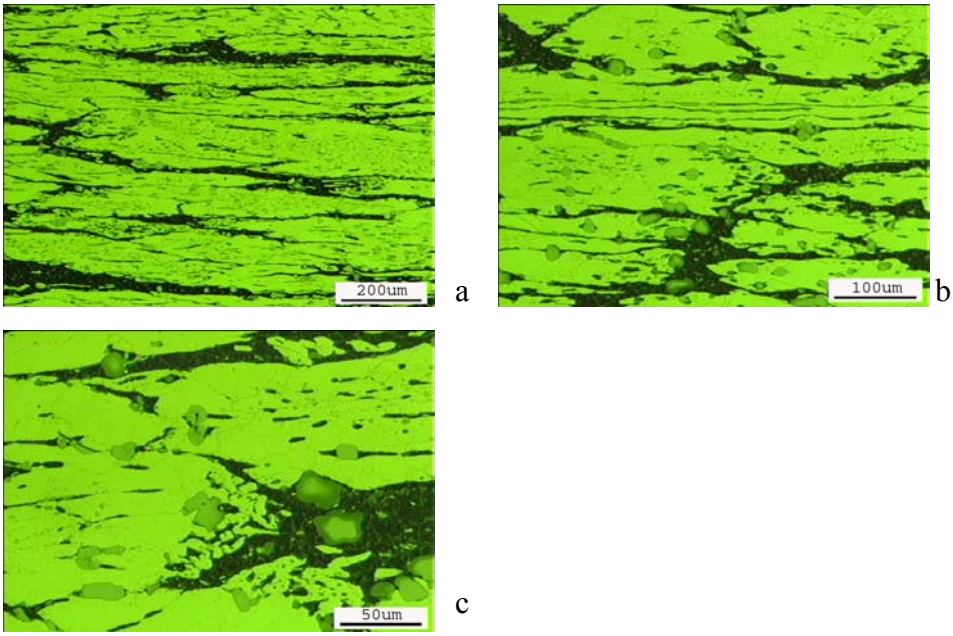

Figure A.9: The following micrographs (a through c) are for magnifications of 290x, 370x, and 750x at 820°C, respectively.

780°C micrographs:

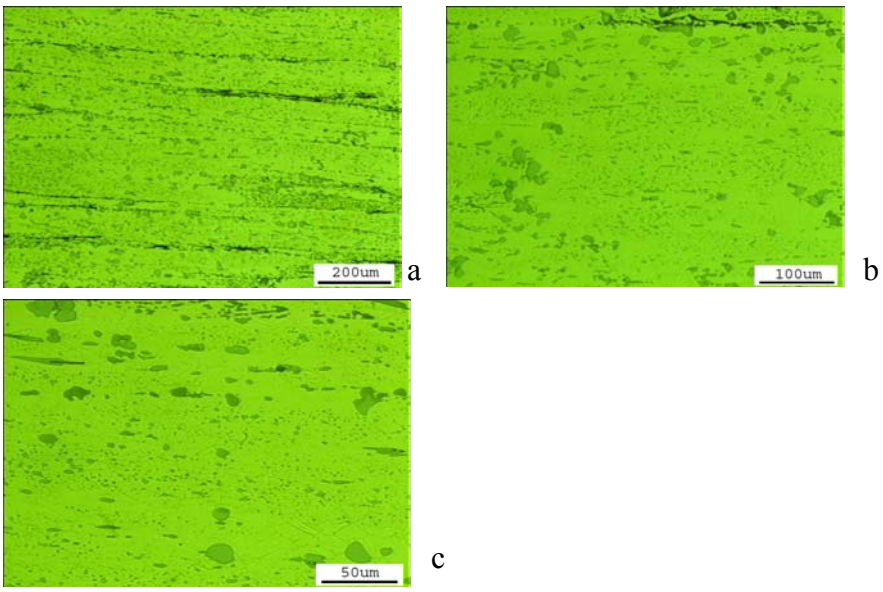

Figure A.10: The following micrographs (a through c) are for magnifications of 290x, 370x, and 750x at 780°C, respectively.

C. ANNEALED 10:1 DEFORMED MICROGRAPHS:

1000°C micrographs:

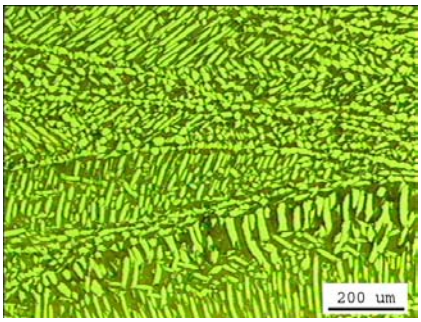

a

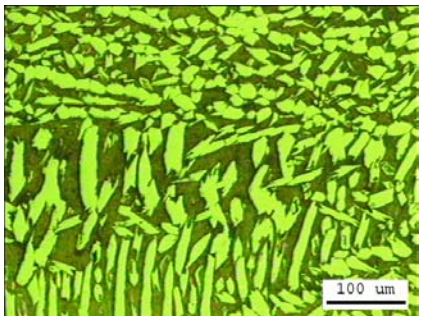

b

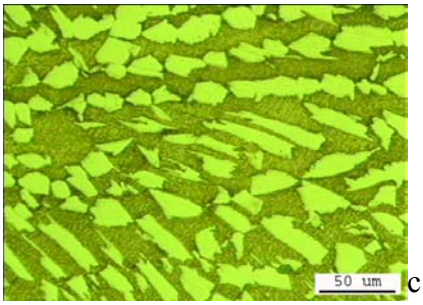

c

Figure A.11: The following micrographs (a through c) are for magnifications of 290x, 370x, and 750x at 1000°C, respectively.

900°C micrographs:

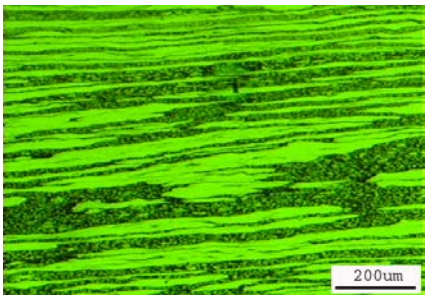

a

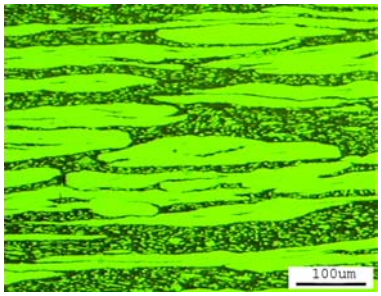

b

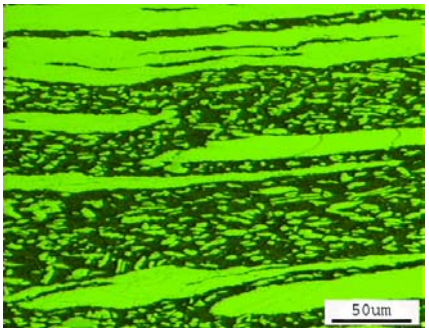

c

Figure A.12: The following micrographs (a through c) are for magnifications of 290x, 370x, and 750x at 900°C, respectively.

870°C micrographs:

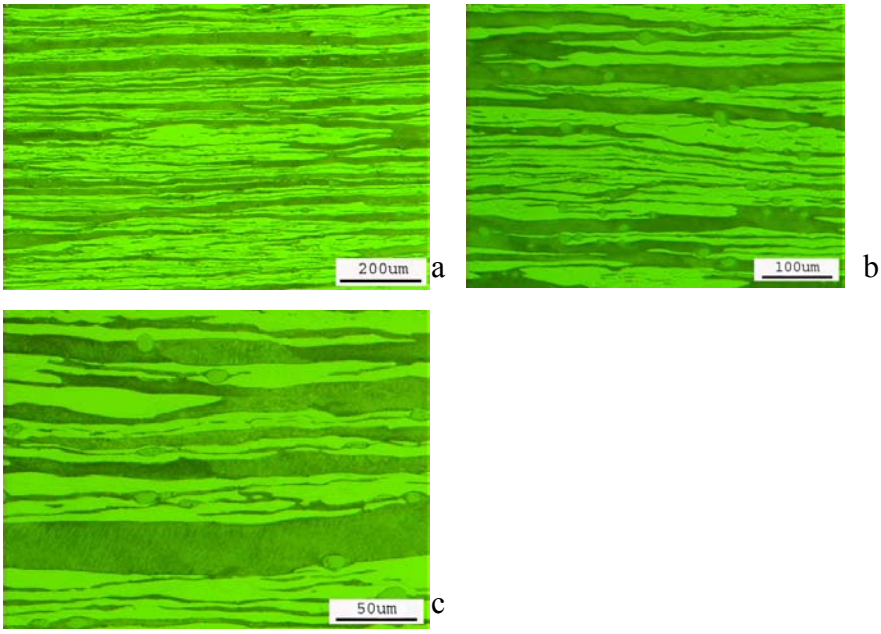

Figure A.13: The following micrographs (a through c) are for magnifications of 290x, 370x, and 750x at 870°C, respectively.

820°C micrographs:

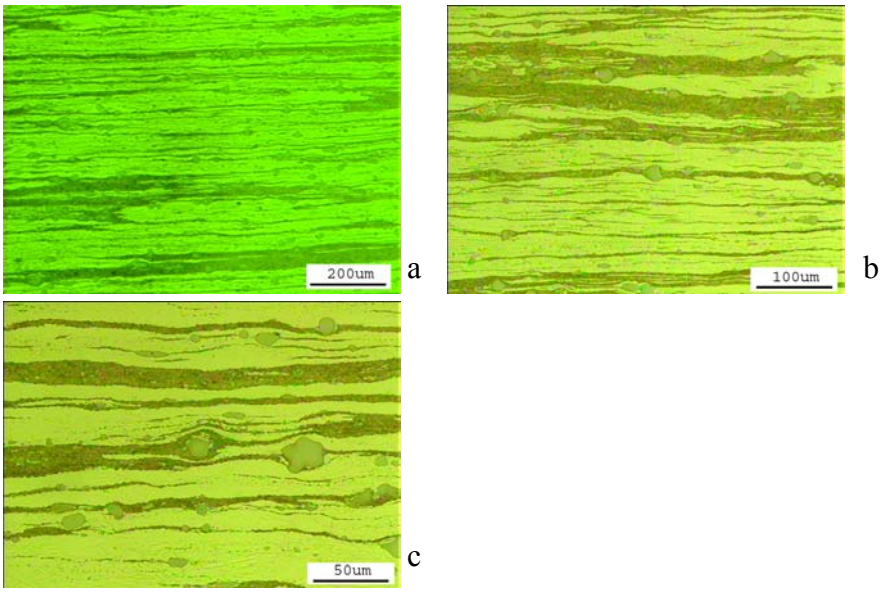

Figure A.14: The following micrographs (a through c) are for magnifications of 290x, 370x, and 750x at 820°C, respectively.

780°C micrographs:

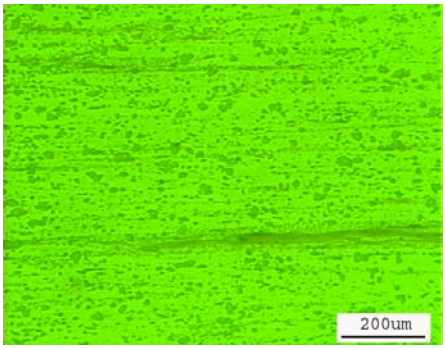

a

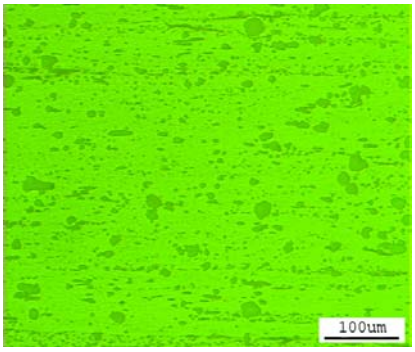

b

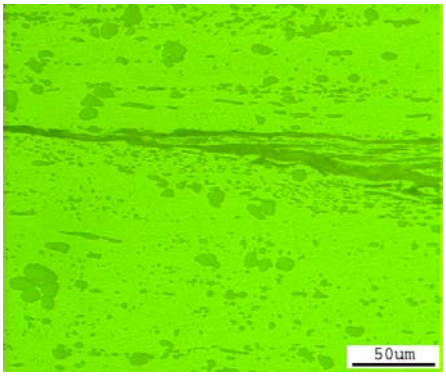

c

Figure A.15: The following micrographs (a through c) are for magnifications of 290x, 370x, and 750x at 780°C, respectively.

APPENDIX B

A. TENSILE SAMPLES:

Figure B.1a-c shows the size, shape and condition of the tensile samples. Notice that the 820°C shows a moderate amount of bending.

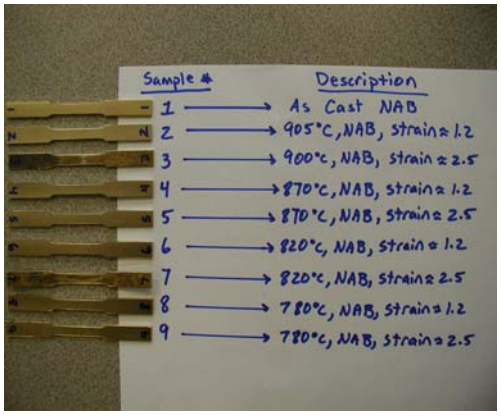

a

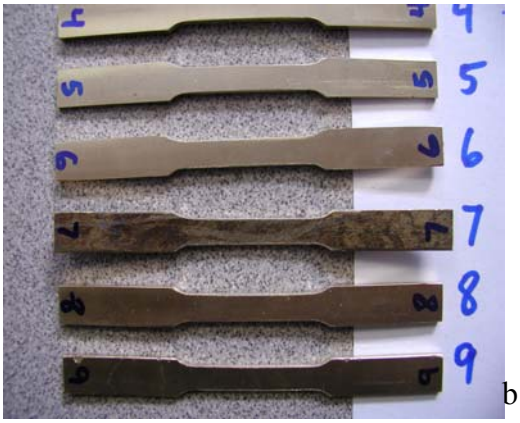
b

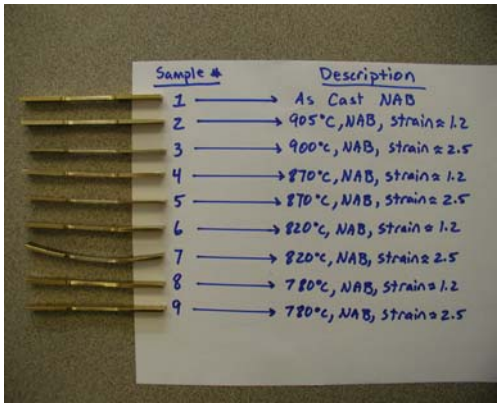

c

Figure B.1: Side and top views of the tensile samples.

THIS PAGE INTENTIONALLY LEFT BLANK

APPENDIX C

A. MATLAB CODE FOR PIXEL COUNT:

The following code was used to perform the pixel count of a monochrome picture of transformed beta. 480*640 represents the picture size in pixels.

```
A = imread('File Name','bmp');

image(A)

imagesc(A,[0,1]); colormap(gray)

A(1,:);

perc=(sum(sum(A))/(480*640))*100
```

THIS PAGE INTENTIONALLY LEFT BLANK

APPENDIX D

A. PERCENTAGES OF ALPHA AND BETA

1 hr Annealed NAB and then Air Cooled to ambient		
Temperature ^{o}C	% Alpha	% Beta
770	98.1	1.9
820	88.2	11.8
870	61.6	38.4
910	38.3	61.7
950	19.4	80.6

Table D.1: Percentage of Alpha and Beta of an As-Cast NAB sample. (Note: Kappa 2 and 4 were consolidated into the alpha and beta matrix)

1 hr annealed NAB, rolled to a 3.5:1 reduction and then air-cooled to ambient		
Temperature ^{o}C	% Alpha	% Beta
780	97.0	3.0
820	74.8	25.2
870	53.4	46.6
905	50.0	50.0
1000	1.0	99

Table D.2: Percentage of Alpha and Beta of a 3.5:1 reduced NAB sample. (Note: Kappa 2 and 4 were consolidated into the alpha and beta matrix)

1 hr annealed NAB, rolled to a 10:1 reduction and then air-cooled to ambient		
Temperature ^{o}C	% Alpha	% Beta
780	97.6	2.4
820	78.0	22.0
870	65.1	34.9
900	44.0	56.0
1000	56.7	43.3

Table D.3: Percentage of Alpha and Beta of a 10:1 reduced NAB sample. (Note: Kappa 2 and 4 were consolidated into the alpha and beta matrix.)

THIS PAGE INTENTIONALLY LEFT BLANK

LIST OF REFERENCES

1. Duma, J.A., "Heat Treatments For Optimizing Mechanical and Corrosion Resisting Properties of Nickel-Aluminum Bronzes," *Naval Engineers Journal*, v. 87, p. 45-64,1975.

2. Metals Handbook, 9th Ed., v. 2, Properties & Selections: Nonferrous Alloys and Pure Metals.

3. Military Specifications For Bronze, Nickel-Aluminum (UNS C95800), Castings for Seawater Service (MIL-B-24480A), 20 June 1985.

4. American Society for Testing and Materials (ASTM) B148 – 93a, Standard Specification for Aluminum-Bronze Sand Castings.

5. Sahoo, M., "Structure and Mechanical Properties of Slow-Cooled Nickel-Aluminum Bronze Alloy C95800," *AFS Trans*, v. 90, p. 913-926, 1982.

6. Wenschot, P., "The Properties of Ni-Al Bronze Sand Cast Ship Propellers in Relation to Section Thickness," *International Shipbuiling Progress*, v. 34, p.112-123,1987.

7. Ferrara, R.J. and Caton, T.E., "Review of Dealloying of Cast Aluminum Bronze and Nickel-Aluminum Bronze Alloys in Sea Water Service," *Materials Performance*, v. 21, No. 2, p. 30-34, 1982.

8. G.W. Lorimer, F. Hasan, J. Iqbal, N. Ridley, "Observation of Microstructure and Corrosion Behavior of Some Aluminum Bronzes," *British Corrosion Journal*, v. 21, p. 244-248, 1986.

9. Culpan, E.A. and Rose, G., "Corrosion Behaviour of Cast Nickel Aluminium Bronze in Sea Water," *British Corrosion Journal,* v. 14, p. 160-166, 1979.

10. A.M. Cuevas, MS Thesis, "Microstructure Characterization of Friction-Stir Processed Nickel-Aluminum Bronze through Orientation Imaging Microscopy," Naval Postgraduate School, Monterey, CA, 2002.

11. W.M. Thomas, E.D. Nicholas, J.C. Needham, M.G. Murch, P. Templesmith and C.J. Dawes, "Friction Stir Butt Welding," G.B. Patent Application No. 9125978.8, Dec. 1991; U.S. Patent No. 5460317, Oct. 1995.

12. Mishra, R.S. and Mahoney, M.W., "Friction Stir Processing: A New Grain Refinement Technique to Achieve High Strain Rate Superplasticity in Commercial Alloys," *Materials Science Forum,* v. 357-359, p. 507-514, 2001.

13. P.B. Berbon, W.H. Bingel, R.S. Mishra, C.C. Bampton and M.W. Mahoney, "Friction Stir Processing: A Tool to Homogenize Nanocomposite Aluminum Alloys," *Scripta Materialia*, v. 44, p. 61-66, 2001.

14. R.S. Mishra, M.W. Mahoney, S.X. McFadden, N.A. Mara and A.K. Mukherjee, "High Strain Rate Superplasticity In A Friction Stir Processed 7075 Al Alloy," *Scripta Materialia*, v. 42, p. 163-168, 2000.

15. Weston, G.M., "Survey of Nickel-Aluminium-Bronze Casting Alloys on Marine Applications," Australia Dept. of Defence Report, DSTO MRL, Melbourne, Victoria, MRL-R-807, 1981.

16. Culpan, E.A. and Rose, G., "Microstructural Characterization Of Cast Nickel Aluminium Bronze," *Journal of Materials Science*, v. 13, p. 1647-1657, 1978.

17. F. Hasan, A. Jahanafrooz, G.W. Lorimer and N. Ridley, "The Morphology, Crystallography, and Chemistry of Phases in As-Cast Nickel-Aluminum Bronze," *Met. Trans A*, v. 13a, p.1337-1345, 1982.

18. A. Jahanafrooz, F. Hasan, G.W. Lorimer and N. Ridley, "Microstructural Development in Complex Nickel-Aluminum Bronze," *Met. Trans A*, v. 14a, p. 1951-1956, 1983.

19. D.E. Bell, MS Thesis, "Microstructural Development and Corrosion Resistance of Laser-Welded Nickel-Aluminum Bronze," Pennsylvania State University, PA, 1994.

20. Jesse Sherburn, Intern for Prof. T. McNelley, Naval Postgraduate School, summer 2003.

21. Brezina, P, "Heat Treatment of Complex Aluminum Bronzes," *Int. Met. Rev*., v. 27, n. 2, p. 77-120, 1982.

22. M.A. Ballou, MS Thesis: "The Effect of Thermomechanical Processing on the Tensile Properties and Microstructure of a 6061 Al-Al_2O_3 Metal Matrix Composite." Naval Postgraduate School, Monterey, CA, 1995

23. G.E. Dieter "Mechanical Metallurgy" 3rd Edition. p. 586-615.

24. National Center for Excellence in Metalworking Technology: Atlas of Formability – Cast Ni-Al Bronze, 1995

25. W. Nabach, MS Thesis, "The Effects of Isothermal Deformation and Annealing on the Microsructure of Nickel-Aluminum-Bronze Propeller Material," Naval Postgraduate School, Monterey, CA, 2003.

26. R.S. Mishra, "Friction Stir Processing Technologies," *Advanced Materials and Processes*, p.43-46, October 2003.

THIS PAGE INTENTIONALLY LEFT BLANK

INITIAL DISTRIBUTION LIST

1. Defense Technical Information Center
   Ft. Belvoir, Virginia

2. Dudley Knox Library
   Naval Postgraduate School
   Monterey, California

3. Professor Terry McNelley
   Naval Postgraduate School
   Dept. of Mechanical Engineering
   Monterey, California

4. Professor A. J. Healey
   Naval Postgraduate School
   Dept. of Mechanical Engineering
   Monterey, California

5. CDR S. Cunningham
   Naval Postgraduate School
   Dept. of Mechanical Engineering
   Monterey, California

6. Murray W. Mahoney
   Rockwell Science Center
   1049 Camino Dos Rios
   Thousand Oaks, California 91360

7. William Palko
   Naval Surface Warfare Center
   Caderock Division
   9500 MacArthur Boulevard
   West Bethesda, Maryland 20817-5700

8. Dr. Leo Christodoulou
   DARPA/DSO
   3701 North Fairfax Drive
   Arlington, Virginia 22203-1714